

Hwiccewurm trispiculum gen. et sp. nov., a new leptopleuronine procolophonid from the Late Triassic of southwest England

Butler, Richard; Meade, Luke; Cleary, Terri; McWhirter, Kai; Brown, Emily; Kemp, Tom; Benito, Juan; Fraser, Nicholas

DOI:
[10.1002/ar.25316](https://doi.org/10.1002/ar.25316)

License:
Creative Commons: Attribution (CC BY)

Document Version
Publisher's PDF, also known as Version of record

Citation for published version (Harvard):
Butler, R, Meade, L, Cleary, T, McWhirter, K, Brown, E, Kemp, T, Benito, J & Fraser, N 2023, 'Hwiccewurm trispiculum gen. et sp. nov., a new leptopleuronine procolophonid from the Late Triassic of southwest England', *The Anatomical Record*. <https://doi.org/10.1002/ar.25316>

[Link to publication on Research at Birmingham portal](#)

General rights

Unless a licence is specified above, all rights (including copyright and moral rights) in this document are retained by the authors and/or the copyright holders. The express permission of the copyright holder must be obtained for any use of this material other than for purposes permitted by law.

- Users may freely distribute the URL that is used to identify this publication.
- Users may download and/or print one copy of the publication from the University of Birmingham research portal for the purpose of private study or non-commercial research.
- User may use extracts from the document in line with the concept of 'fair dealing' under the Copyright, Designs and Patents Act 1988 (?)
- Users may not further distribute the material nor use it for the purposes of commercial gain.

Where a licence is displayed above, please note the terms and conditions of the licence govern your use of this document.

When citing, please reference the published version.









Take down policy

While the University of Birmingham exercises care and attention in making items available there are rare occasions when an item has been uploaded in error or has been deemed to be commercially or otherwise sensitive.

If you believe that this is the case for this document, please contact UBIRA@lists.bham.ac.uk providing details and we will remove access to the work immediately and investigate.

SPECIAL ISSUE ARTICLE

Hwiccewyrms trispiculum gen. et sp. nov., a new leptopleuronine procolophonid from the Late Triassic of southwest England

Richard J. Butler¹  | Luke E. Meade¹  | Terri J. Cleary¹  |
Kai T. McWhirter¹  | Emily E. Brown^{1,2}  | Tom S. Kemp³  | Juan Benito⁴  |
Nicholas C. Fraser⁵ 

¹School of Geography, Earth & Environmental Sciences, University of Birmingham, Birmingham, UK

²Fossil Reptiles, Amphibians and Birds Section, Natural History Museum, London, UK

³St John's College, University of Oxford, Oxford, UK

⁴Department of Earth Sciences, University of Cambridge, Cambridge, UK

⁵Department of Natural Sciences, National Museums Scotland, Edinburgh, Scotland

Correspondence

Richard J. Butler, School of Geography, Earth & Environmental Sciences, University of Birmingham, Birmingham, UK.

Email: r.butler.1@bham.ac.uk

Abstract

The fissure fill localities of southwest England and South Wales are well-known for preserving rich assemblages of predominantly small-bodied Late Triassic to Early Jurassic tetrapods, but many aspects of these assemblages remain contentious. The age of the Late Triassic fissures is disputed, with some lines of argument suggesting a latest Triassic (Rhaetian) age, whereas other evidence suggests they may be as old as Carnian. The fissures have been hypothesized by some workers to have formed on an archipelago, with island effects invoked to explain aspects of the assemblages such as the abundance of small-bodied species. Procolophonids were a successful group of Triassic parareptiles, best known from Early to early Late Triassic assemblages, but have only recently been described from one of the fissure fill sites (Ruthin) based upon fragmentary remains. Here, we describe new procolophonid specimens from another fissure (Cromhall) that represent at least six individuals of different sizes, with much of the skeleton represented including well-preserved skull material. The Cromhall procolophonid shows strong similarities to Late Triassic procolophonids from Scotland, Brazil and North America, but both autapomorphies and a unique character combination demonstrate that it represents a new species, which we name as *Hwiccewyrms trispiculum* gen. et sp. nov. Phylogenetic analysis places *Hwiccewyrms* in a derived clade within Leptopleuroninae, together with *Leptopleuron*, *Hypsognathus*, and *Soturnia*. The largest specimens of *Hwiccewyrms* demonstrate a body size that is similar to *Leptopleuron* and *Hypsognathus*, supporting other recent work that has questioned the insular dwarfism hypothesis for the fissure fill assemblages.

KEYWORDS

fissure fills, Parareptilia, phylogeny, Procolophonidae, Triassic

Procolophonids were a successful and widespread group of small-bodied parareptiles that originated in the late Permian, appear to have been unaffected by the end-Permian mass extinction event, and subsequently underwent an evolutionary radiation in the Triassic (Cisneros, 2008; Cisneros & Ruta, 2010; MacDougall et al., 2019; Modesto et al., 2001; Ruta et al., 2011; Tsuji & Müller, 2009). Triassic fossils of the group are known from localities worldwide, including Western Europe (Säilä, 2010; Skinner et al., 2020; Spencer, 2000; Spencer & Storrs, 2002; Sues & Reisz, 2008; Zaher et al., 2019), Russia (Ivakhnenko, 1979; Spencer & Benton, 2000), China (Li, 1983, 1989), southern Africa (Carroll & Lindsay, 1985; deBraga, 2003; Falconnet et al., 2012; Modesto et al., 2001; Modesto et al., 2010; Modesto & Damiani, 2003; Tsuji, 2018), North America (Sues et al., 2000; Sues & Baird, 1998), South America (Cisneros & Schultz, 2003; Piñeiro et al., 2004; Pinheiro et al., 2021; Silva-Neves et al., 2020), and Australia (Hamley et al., 2021). The group was most widespread and abundant during the Early Triassic and the early Middle Triassic (Anisian) but is relatively scarce in post-Anisian assemblages (Cisneros, 2008).

The only procolophonid clade known to have survived into the Late Triassic is Leptopleuroninae (Cisneros, 2008), with records described from Brazil (Cisneros & Schultz, 2003), Scotland (Säilä, 2010; Spencer, 2000), North America (Fraser et al., 2005; Small, 1997; Sues et al., 2000; Sues & Baird, 1998) and possibly South Wales (Skinner et al., 2020). The stratigraphically youngest leptopleuronine records occur in rocks of late Norian to Rhaetian age (e.g., Fraser et al., 2005; Sues et al., 2000) and are the latest known surviving members of Parareptilia (Ruta et al., 2011; Tsuji & Müller, 2009).

Rich assemblages of terrestrial vertebrates, mostly small bodied, of Late Triassic age are known from a series of fissure fill deposits in southwest England and south Wales (Fraser, 1994; Halstead & Nicoll, 1971; Robinson, 1957; Whiteside et al., 2016; Whiteside & Marshall, 2008). These fissure deposits have yielded many significant species of mammalianomorph, lepidosauromorph, and archosauromorph tetrapods. Procolophonids have been mentioned as present within the fissure fills (Edwards, 2000; Fraser, 1986a, 1988a, 1988b, 1988c; Fraser, 1994; Halstead & Nicoll, 1971; Skinner et al., 2020; Walkden & Fraser, 1993; Whiteside et al., 2016; Whiteside & Duffin, 2017), and as a clade known to be almost exclusively present in the Triassic have been considered biostratigraphically informative (e.g., Fraser, 1986a, 1986b). However, only relatively incomplete material has been described to date, comprising mostly tooth and jaw fragments (Edwards, 2000; Edwards & Evans, 2006; Fraser, 1986a; Halstead & Nicoll, 1971; Skinner et al., 2020; Whiteside & Duffin, 2017). Here, we describe a new genus and species of leptopleuronine procolophonid from Cromhall Quarry, southwest England, based on well-preserved specimens representing much of the skeleton.

1 | GEOLOGICAL SETTING

The area of southern Wales and southwest England surrounding the Bristol Channel is home to a system of karstic limestone caves and sediment infills, or “fissure fills”, which span the Triassic–Jurassic boundary (Whiteside et al., 2016). Remains of animals preserved within the fissures include many uncommonly recovered small vertebrate fossils (Fraser, 1994; Halstead & Nicoll, 1971; Robinson, 1957; Whiteside et al., 2016; Whiteside & Marshall, 2008). The precise age and environment of deposition of the fissure fills has been the subject of considerable dispute. Some recent work has suggested that all the vertebrate-bearing fills are younger than the Rhaetian transgression (Mussini et al., 2020; Whiteside et al., 2016; Whiteside & Marshall, 2008). However, this remains contentious with other workers arguing for older (Carnian or Norian) ages for some of the fissures (e.g., Simms, 1990; Walkden et al., 2021; Walkden & Fraser, 1993), including based on as-yet-unpublished radiometric dates (Simms & Drost, 2022).

The fossils described here come from Cromhall Quarry (also known as Slickstones Quarry) in South Gloucestershire, England (Figure 1). The age of the fissure deposits at Cromhall is disputed and has been proposed to be either pre-Rhaetian Late Triassic (i.e., Carnian–Norian; Simms, 1990; Walkden & Fraser, 1993; Walkden et al., 2021; Simms & Drost, 2022) or Rhaetian (Morton

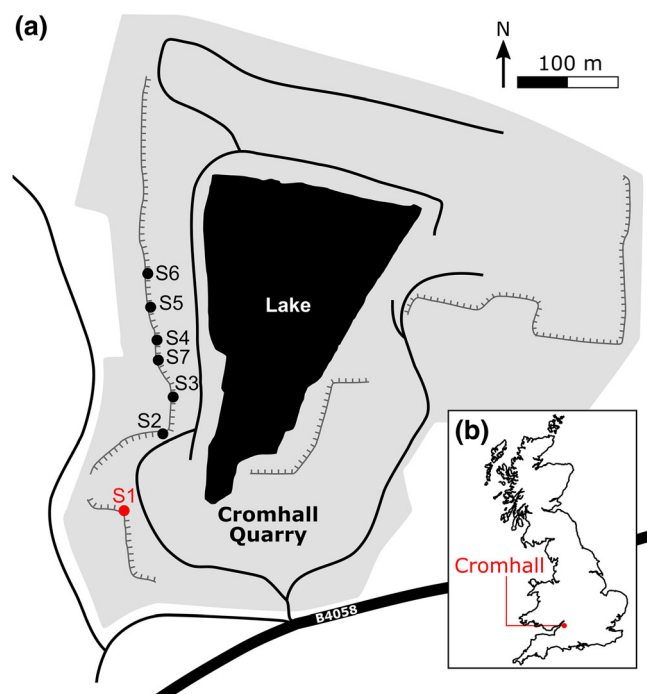


FIGURE 1 Locality map for Cromhall Quarry (a) within the United Kingdom (b). S1–S6 refer to fissures within Cromhall, following the terminology of Walkden and Fraser (1993).

et al., 2017; Mussini et al., 2020; Whiteside et al., 2016; Whiteside & Marshall, 2008). The described terrestrial fauna from here includes the rhynchocephalians *Clevosaurus*, *Diphydontosaurus*, *Pelecymala*, *Sigmala* and *Planocephalosaurus*, drepanosaurids, the gliding reptile *Kuehneosaurus*, an aetosaur, crocodylomorphs, and a dinosauriform (Fraser, 1982, 1985, 1986a, 1986b, 1988a, 1988b, 1988c, 1994; Fraser et al., 2002; Fraser & Renesto, 2005; Fraser & Walkden, 1983, 1984; Halstead & Nicoll, 1971; Lucas et al., 1999; O'Brien et al., 2018; Renesto & Fraser, 2003; Robinson, 1957, 1973; Walkden & Fraser, 1993; Whiteside et al., 2016; Whiteside & Marshall, 2008). Fossils have been collected from more than seven different fissures at Cromhall, which may have formed at distinct times (Walkden & Fraser, 1993). Unlike in many of the other fissures, non-mammaliaform cynodont and mammaliaform fossils are unknown from Cromhall.

The procolophonid specimens described here (registered at the Museum of Zoology, University of Cambridge [UMZC]) were collected by Jeanne Evans, an amateur paleontologist, and were originally studied by her and TSK in the early 1970s. Although details of the collection of the UMZC material are unavailable and original associations between elements are unclear, they were apparently collected from a single small area within Cromhall, possibly from fissure “site 1” or “S1” or at least a continuation of that feature that has since been quarried away (Figure 1; Walkden & Fraser, 1993; Edwards, 2000), part of faunal assemblage C of Walkden and Fraser (1993). This inference is supported by the presence in the University of Aberdeen (AUP) collections of paired frontals (AUP 11308; Figure 6) from site 1 of Walkden and Fraser (1993), that show a similar size and near-identical morphology to a frontal within the UMZC material (UMZC 2023.4.8). We tentatively refer these paired frontals to our new taxon. Site 1 is inferred to be the youngest of the exposed fissures at Cromhall, and has also yielded material of *Clevosaurus*, *Diphydontosaurus* and crocodylomorphs (Fraser, 1988a, 1994; Walkden & Fraser, 1993). Specimens most probably from the vicinity of site 1 held by UMZC were collected from a light buff-colored limestone and prepared mostly using acid digestion (Fraser, 1988a). The procolophonid specimens represent multiple individuals (at least six) of different sizes.

2 | METHODS

CT scanning was conducted at the XTM Facility, Palaeobiology Research Group, University of Bristol using a Nikon XTH 225ST X-ray tomography scanner. Scan parameters were set at: 190 kV and 155 μ A for

specimens UMZC 2023.4.1 and UMZC 2023.4.18, yielding 2000 TIF images of 0.031 mm voxel size; 150 kV and 183 μ A for specimens UMZC 2023.4.2, UMZC 2023.4.19, and UMZC 2023.4.20, yielding 1930 TIF images of 0.029 mm voxel size; and 170 kV and 190 μ A for all other scanned specimens, yielding 1970 TIF images of 0.081 mm voxel size. The CT image files were imported into Avizo 3D (version 2021.2) for segmentation and the resulting 3D surface models were visualized and rendered in Blender (version 3.0.1). Data and models are available at Morphosource (<https://www.morphosource.org/projects/000530765?locale=en>).

We incorporated *Hwiccewyrms trispiculum* into the cladistic character/taxon matrix of Hamley et al. (2021), which represents a modified version of the dataset of Cisneros (2008). The Hamley et al. (2021) dataset includes 32 taxa and 66 characters, and it was possible to score *H. trispiculum* for 60% of the latter. Analyses were run in TNT 1.6 for MacOS (Goloboff & Morales, 2023), primarily following the protocols in Hamley et al. (2021). *Nyctiphruretus* was used to root the tree. Hamley et al. (2021) ran three separate phylogenetic analyses, which we replicated here for comparability. Analysis 1 used equal character weights. Analysis 2 used implied weightings against homoplasy (Goloboff et al., 2008) with the default weight strength ($K = 3$). Analysis 3 used equal weights but excluded *Pintosaurus magnidentis* due to the high levels of missing data. For each analysis, we first used a new technology search with 100 random addition sequences. The recovered trees were saved to RAM and used as the basis for a traditional search using the tree bisection and reconnection (TBR) swapping algorithm. Bootstrap analyses were run using 10,000 replicates, a traditional search and reported using absolute frequencies. The phylogenetic dataset is provided as supplementary material S1.

3 | SYSTEMATIC PALAEOLOGY

Parareptilia Olson, 1947 sensu Laurin & Reisz (1995)

Procolophonoidea Romer, 1956

Procolophonidae Seeley, 1888

Leptopleuroninae Ivakhnenko, 1979

Hwiccewyrms trispiculum gen. et sp. nov. (Figures 2–15).

“isolated procolophonid remains”; Fraser, 1988a:129.

“procolophonid”; Fraser, 1988b:567.

“Cromhall procolophonid”; Fraser, 1988c:135.

“procolophonid”; Walkden & Fraser, 1993:Figure 7b, d, e.

“procolophonid b”; Fraser, 1994:Figure 11.5.

“procolophonid b”; Edwards, 2000:48.

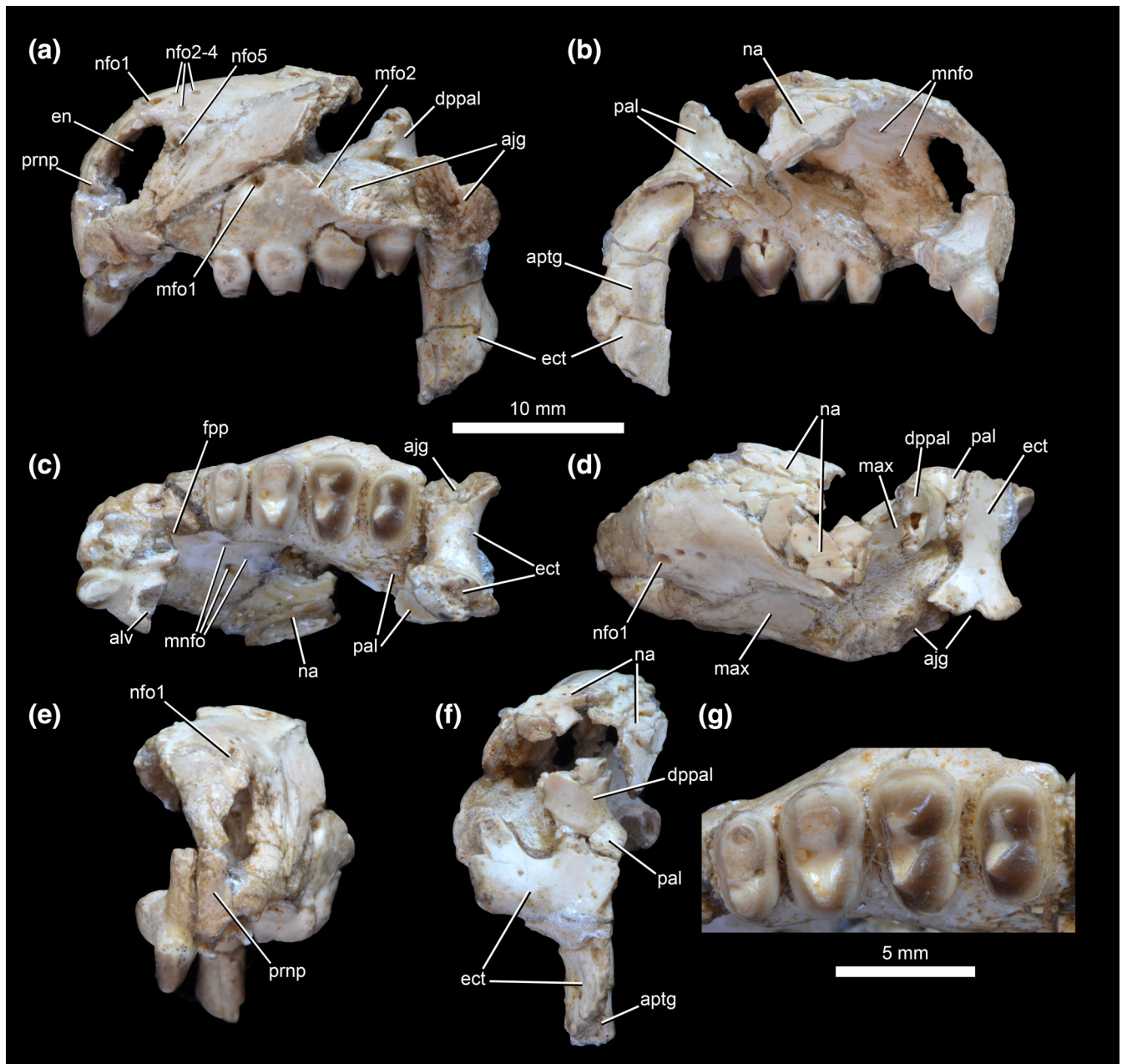


FIGURE 2 *Hwiccewurm trispiculum* gen et sp. nov. UMZC 2023.4.1 (holotype), anterior portion of the skull, photographs in left lateral (a), right lateral (b), ventral (c), dorsal (d), anterior (e) and posterior (f) views, with close-up of left maxillary tooth row in occlusal view (g). ajg, articulation surfaces on maxilla and ectopterygoid for the jugal; alv, alveolus; aptg, articular surface on the ectopterygoid for the pterygoid; dppal, dorsal process of the palatine; ect, ectopterygoid; en, external naris; fpp, foramen prepalatinum; max, maxilla; mfo1, mfo2, foramina on the lateral surface of the maxilla; mnfo, foramina on the medial surface of the nasal; na, nasal; nfo1, nfo2-4, nfo5, foramina on the lateral surface of the nasal; pal, palatine; prnp, prenarial process of the premaxilla.

“a procolophonid, possibly *Hypsognathus*”; Whiteside et al., 2016:283.

Holotype: UMZC 2023.4.1, articulated anterior portion of skull, including left premaxilla, fragments of right premaxilla, left maxilla, left nasal, fragments of right nasal, left ectopterygoid (Figures 2–3; Walkden & Fraser, 1993, Figure 7d).

Referred material: UMZC 2023.4.2, complete right premaxilla in articulation with right maxilla (Figure 4i–k); UMZC 2023.4.3, left premaxilla (Figure 4a, b, e); UMZC 2023.4.4, partial right premaxilla, maxilla and nasal (Figure 4c, d, h); UMZC 2023.4.5, partial left maxilla (Figure 4g); UMZC 2023.4.6, partial left maxilla (Figure 4l); UMZC 2023.4.7, partial right maxilla (Figure 4f); UMZC

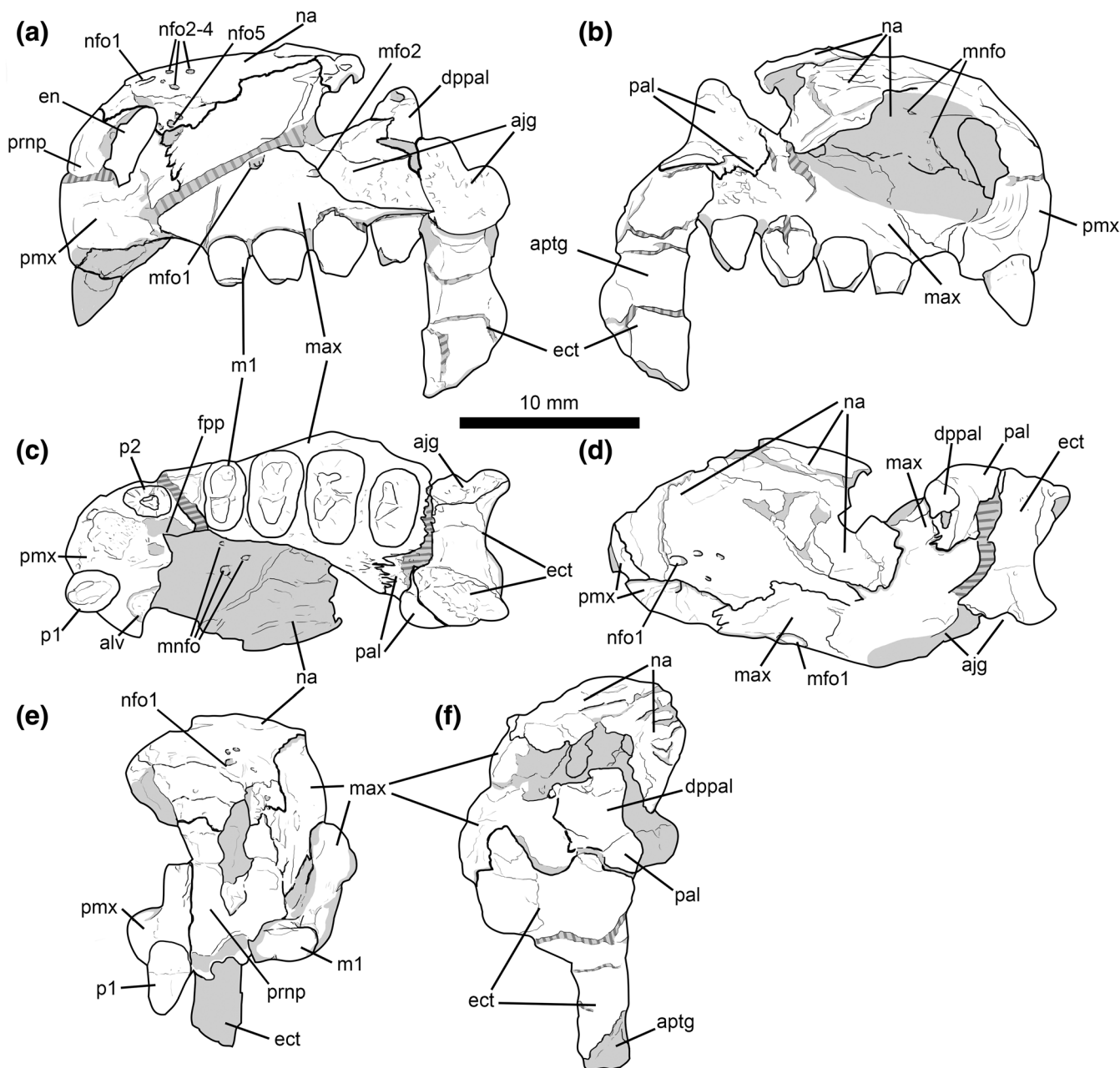


FIGURE 3 *Hwiccewyrn trispiculum* gen et sp. nov. UMZC 2023.4.1 (holotype), anterior portion of the skull, line drawings in same views as for Figure 2. ajg, articulation surfaces on maxilla and ectopterygoid for the jugal; alv, alveolus; aptg, articular surface on the ectopterygoid for the pterygoid; dppal, dorsal process of the palatine; ect, ectopterygoid; en, external naris; fpp, foramen prepalatinum; m1, first maxillary tooth; max, maxilla; mfo1, mfo2, foramina on the lateral surface of the maxilla; mnfo, foramina on the medial surface of the nasal; na, nasal; nfo1, nfo2-4, nfo5, foramina on the lateral surface of the nasal; p1, first premaxillary tooth; p2, second premaxillary tooth; pal, palatine; pmx, premaxilla; prnp, prenarial process of the premaxilla.

2023.4.8, left frontal (Figure 5a, b); AUP 11308, paired frontals (Figure 6); UMZC 2023.4.9, partial left and right parietals (Figure 5c, g); UMZC 2023.4.10, partial right parietal (Figure 5d; no 3D model); UMZC 2023.4.11, left supratemporal (Figure 5l, o, p); UMZC 2023.4.12, right supratemporal (Figure 5m, n, q); UMZC 2023.4.13, left jugal, quadratojugal and fragment of quadrate (Figure 5h, i); UMZC 2023.4.14,

partial left quadratojugal; UMZC 2023.4.15, partial left quadratojugal (Figure 5j, l); UMZC 2023.4.16, partial right quadratojugal; UMZC 2023.4.17, partial right jugal (Figure 5e, f); UMZC 2023.4.18, articulated partial braincase (Figure 7); UMZC 2023.4.19, left dentary (Figure 8h-j); UMZC 2023.4.20, left dentary (Figure 8a-c); UMZC 2023.4.21, left dentary (Figure 8d, e); UMZC 2023.4.22, left dentary (Figure 8k, l); UMZC

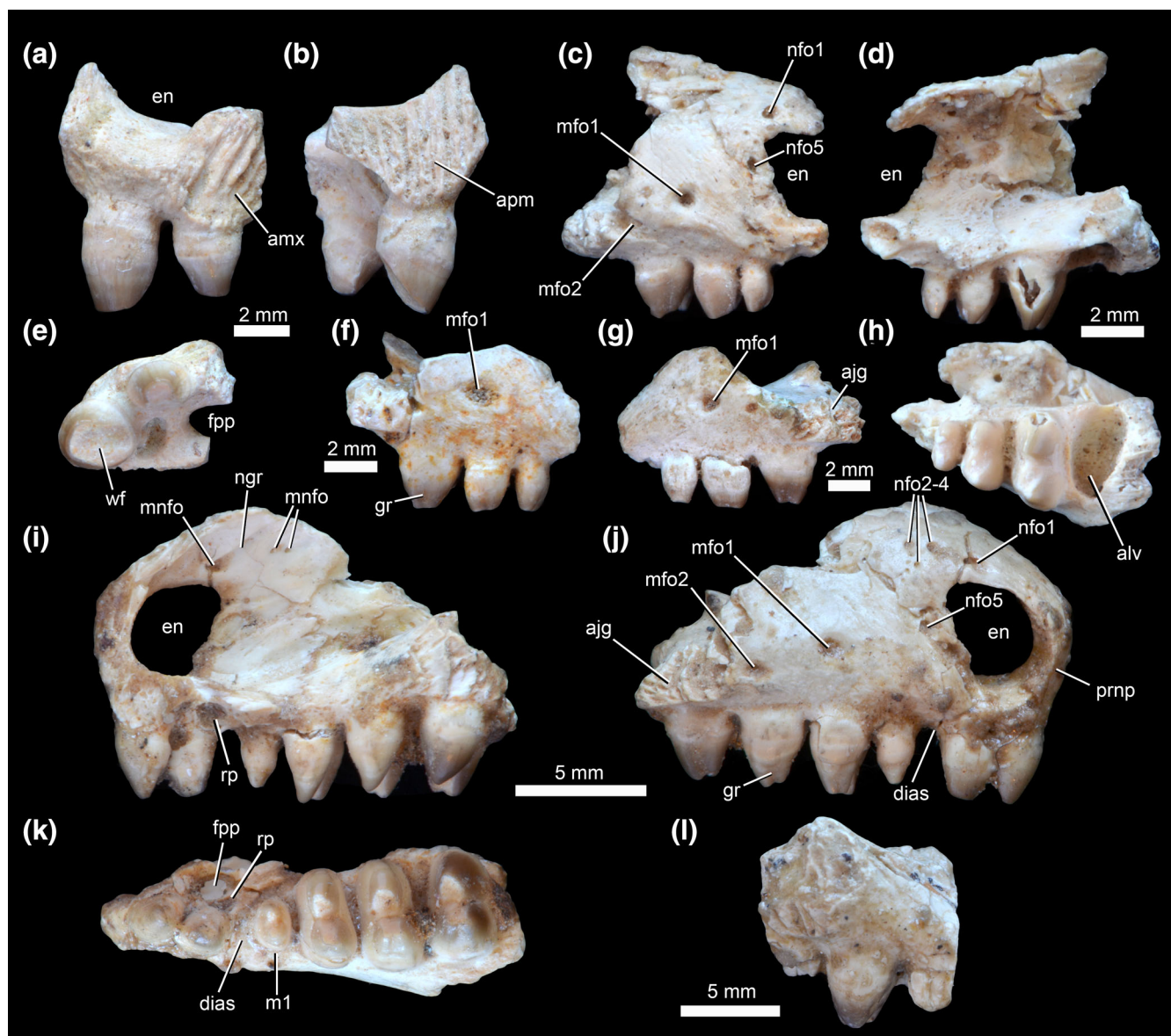


FIGURE 4 *Hwiccewurm trispiculum* gen et sp. nov., anterior portions of the skull, referred specimens. (a, b, e) UMZC 2023.4.3, partial left premaxilla in lateral (a), medial (b) and ventral (e) views. (c, d, h) UMZC 2023.4.4, partial right premaxilla, maxilla and nasal in lateral (c), medial (d) and ventral (h) views. (f) UMZC 2023.4.7, partial right maxilla in lateral view. (g) UMZC 2023.4.5, partial left maxilla in lateral view. (i–k) UMZC 2023.4.2, right premaxilla, maxilla and partial nasal in medial (i), lateral (j) and ventral (k) views. (l) UMZC 2023.4.6, partial left maxilla in medial view. ajg, articulation surface on maxilla for the jugal; alv, alveolus; amx, articulation surface on premaxilla for the maxilla; apm, articulation surface on premaxilla for the opposing premaxilla; dias, diastema between premaxillary and maxillary teeth; en, external naris; fpp, foramen prepalatinum; gr, apicobasally extending groove on lingual surface of maxillary teeth; m1, first maxillary tooth; mfo1, mfo2, foramina on the lateral surface of the maxilla; mnfo, foramina on medial surface of nasal; nfo1, nfo2–4, foramina on the lateral surface of the nasal; ngr, groove on the medial surface of nasal; prnp, prenarial process of the premaxilla; rp, resorption pit; wf, wear facet on first premaxillary tooth.

2023.4.23, left dentary (Figure 8f); UMZC 2023.4.24, fragment of left dentary (Figure 8g); UMZC 2023.4.25, right dentary (Figure 8m); UMZC 2023.4.26, fragment of right dentary (Figure 8n); UMZC 2023.4.27, fragment of right dentary (no 3D model); UMZC 2023.4.28, fragment of right dentary (no 3D model); UMZC 2023.4.29, posterior section of left mandible (Figure 8o–q); UMZC 2023.4.30, cervical centrum

(Figure 10a–f); UMZC 2023.4.31, complete dorsal vertebra (Figure 10m–r); UMZC 2023.4.32, complete dorsal vertebra (Figure 10s–x); UMZC 2023.4.33, dorsal neural arch (Figure 10y–AD); UMZC 2023.4.34, dorsal centrum (Figure 10g–l); UMZC 2023.4.35, left rib (Figure 11a, b; no 3D model); UMZC 2023.4.36, left rib (Figure 11c, d; no 3D model); UMZC 2023.4.37, right rib (Figure 11e, f; no 3D model); UMZC

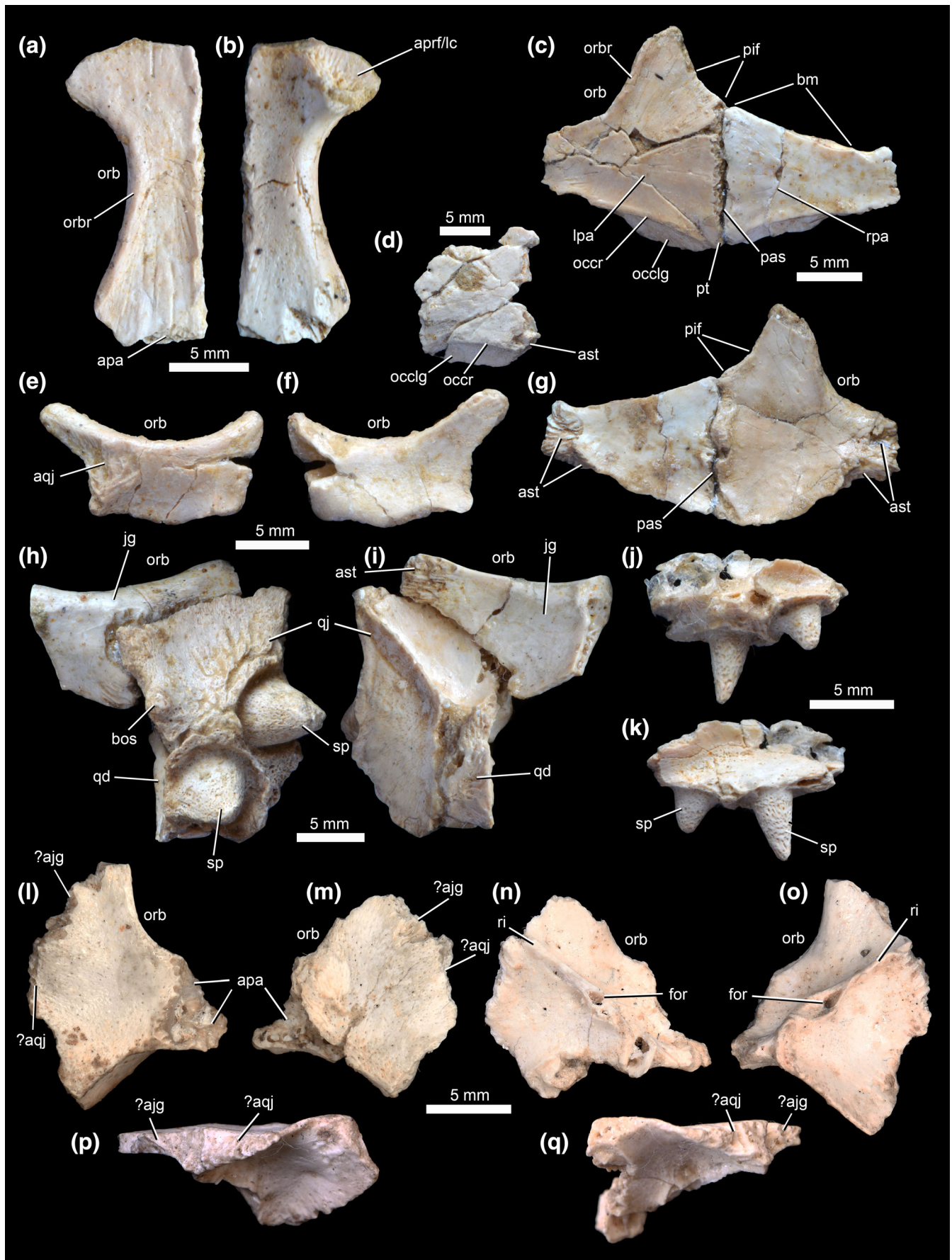


FIGURE 5 Legend on next page.

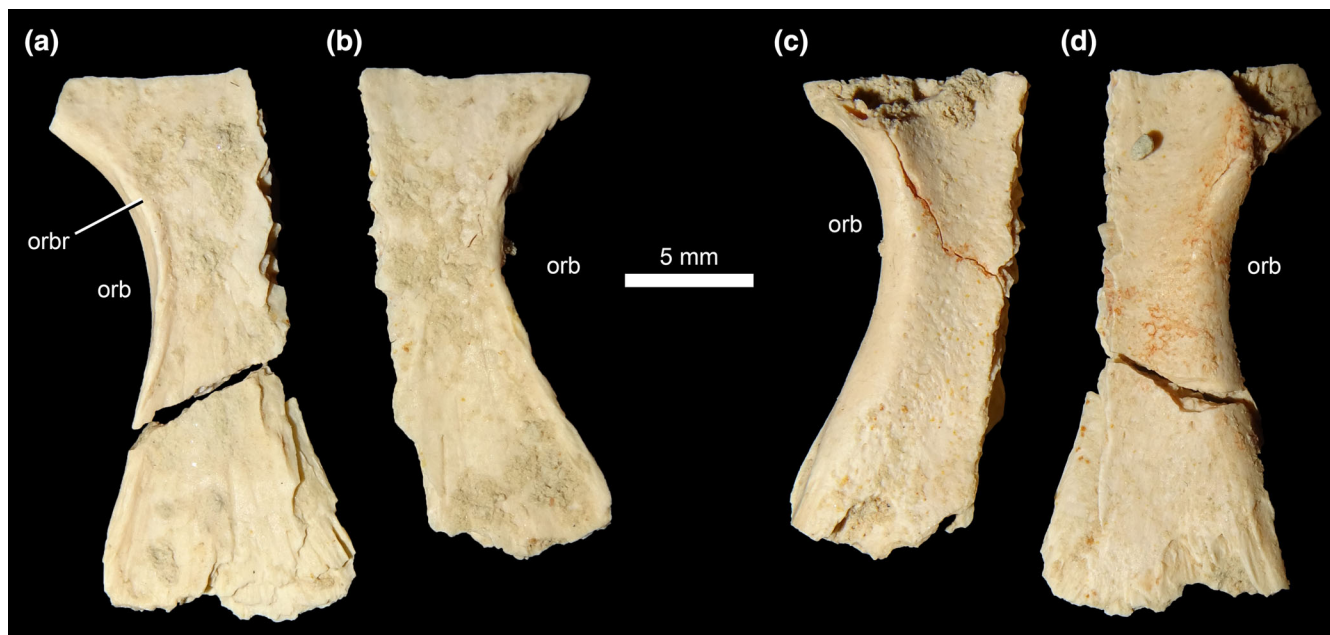


FIGURE 6 *Hwiccewyrms trispiculum* gen et sp. nov., AUP 11308, paired left (a, d) and right (b, c) frontals in dorsal (a, b) and ventral (c, d) views. orb, position of the orbitotemporal fenestra; orbr, thickened rim of the orbitotemporal fenestra.

2023.4.38, right rib (Figure 11g, h; no 3D model); UMZC 2023.4.39, interclavicle (Figure 12a, b); UMZC 2023.4.40, right scapula (Figure 12c–e); UMZC 2023.4.41, left metacoracoid (Figure 12f–h); UMZC 2023.4.42, left humerus (Figure 13a–f; Walkden & Fraser, 1993, Figure 7b, e); UMZC 2023.4.43, left humerus (Figure 13g–l); UMZC 2023.4.44, partial left humerus; UMZC 2023.4.45, left radius (Figure 13m–r); UMZC 2023.4.46, left ilium (Figure 14a, b); UMZC 2023.4.47, left ilium (Figure 14c, d); UMZC 2023.4.48, right ilium (Figure 14e, f); UMZC 2023.4.49, left ischium (Figure 14g–i); UMZC 2023.4.50, left femur (Figure 15a–f); UMZC 2023.4.51, right femur (Figure 15g–l).

Diagnosis: Leptopleuronine procolophonid diagnosed by the following unique combination of characters

(* indicates autapomorphies): four maxillary teeth; all maxillary teeth are molariform and bi- or tricuspid (no anterior monocuspid teeth); m2–m4 are tricuspid with apicobasally extending grooves on the labial surfaces*; small accessory boss on anterior margin of quadratojugal (distinct from typical quadratojugal spines present in *Hwiccewyrms* and other leptopleuronines)*; supratemporal forms the posterolateral corner of the infratemporal fenestra; dentary teeth are subtly bicuspid and not transversely expanded; diastema present between first and second dentary teeth in larger specimens*.

Type locality and horizon: UMZC material is possibly from Site 1, Cromhall Quarry (=Slickstones Quarry), South Gloucestershire, England (Figure 1;

FIGURE 5 *Hwiccewyrms trispiculum* gen et sp. nov., skull elements, referred specimens. (a, b) UMZC 2023.4.8, left frontal in dorsal (a) and ventral (b) views. (c, g) UMZC 2023.4.9, partial left and right parietals in dorsal (c) and ventral (g) views. (d) UMZC 2023.4.10, partial right parietal in dorsal view. (e, f) UMZC 2023.4.17, partial right jugal in lateral (e) and medial (f) views. (h, i) UMZC 2023.4.13, left quadratojugal, partial left jugal, and fragment of left quadrate in lateral (h) and medial (i) views. (j, k) UMZC 2023.4.15, partial left quadratojugal in medial (j) and lateral (k) views. (l, o, p) UMZC 2023.4.11, left supratemporal in dorsal (l), ventral (o), and lateral (p) views. (m, n, q) UMZC 2023.4.12, right supratemporal in dorsal (m), ventral (n), and lateral (q) views. ajg, articulation surface on supratemporal for the jugal; apa, articulation surface on frontal and supratemporal for parietal; aprf/lc, articulation surface on frontal for prefrontal and/or lacrimal; aqj, articulation surface on jugal and supratemporal for the quadratojugal; ast, articulation surface on the parietal for the supratemporal; bm, broken margin; bos, boss on anterior margin of quadratojugal; for, foramen in ventral ridge of supratemporal; jg, jugal; lpa, left parietal; occlg, occipital ledge; occr, ridge along posterior margin of parietal, above occipital ledge; orb, position of the orbitotemporal fenestra; orbr, thickened rim of the orbitotemporal fenestra; pas, midline suture between the parietals; pif, preserved margin of the pineal foramen; pt, midline point along posterior margin of paired parietals; qd, quadrate; qj, quadratojugal; ri, ridge on ventral surface of supratemporal; rpa, right parietal; sp, quadratojugal spine.

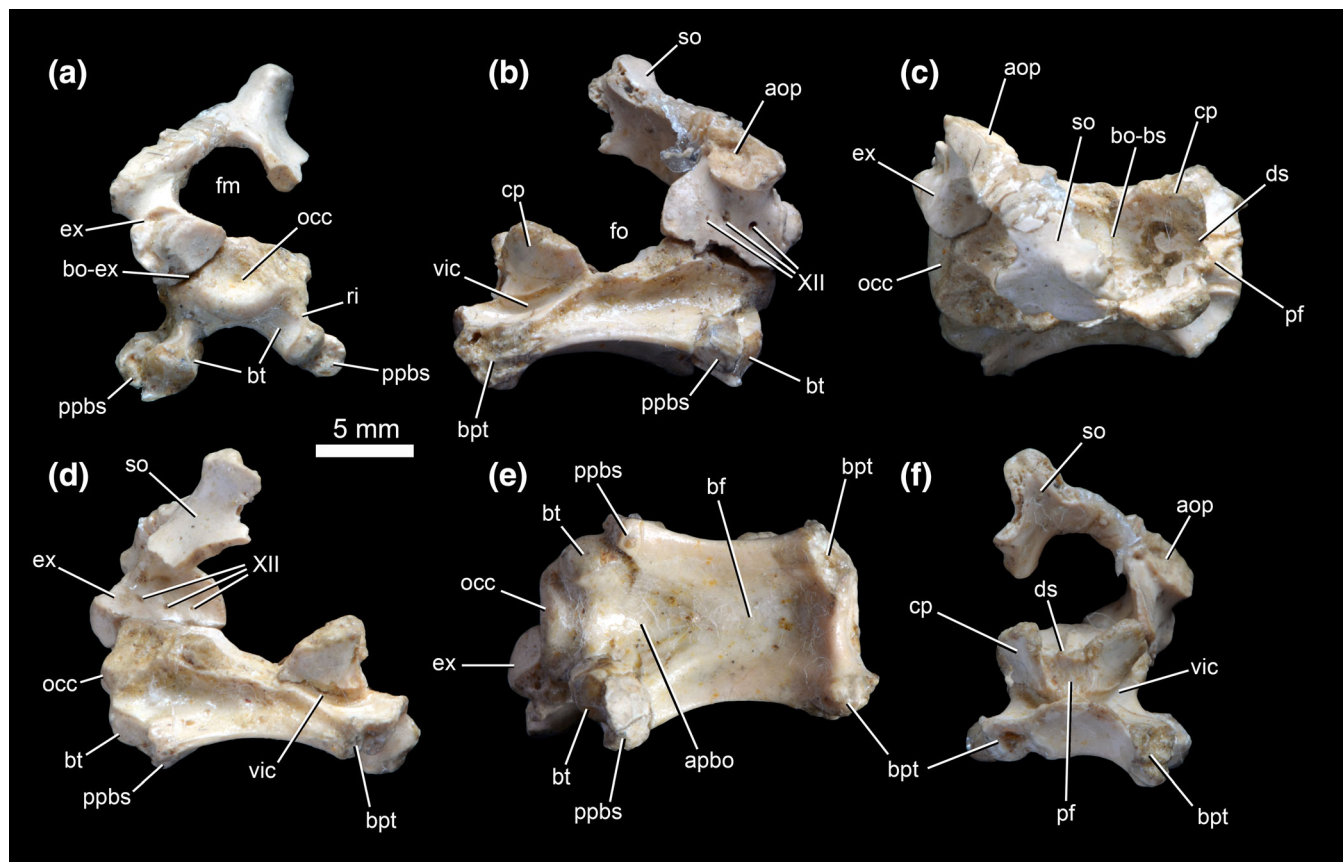


FIGURE 7 *Hwiccewurm trispiculum* gen et sp. nov., UMZC 2023.4.18, partial braincase, referred specimen, in posterior (a), left lateral (b), dorsal (c), right lateral (d), ventral (e) and anterior (f) views. a.op, articulation surface on exoccipital for opisthotic; apbo, triangular anterior process of basioccipital on ventral surface of braincase; bf, basisphenoid fossa; bo-bs, position of basioccipital-basisphenoid suture; bo-ex, position of the basioccipital-exoccipital suture; bpt, basiptyergoid process; bt, basal tuber; cp, clinoid process; ds, dorsum sellae; ex, exoccipital; fm, foramen magnum; fo, fenestra ovalis; occ, occipital condyle; pf, pituitary fossa; ppbs, posterior process of the basisphenoid; ri, ridge on basioccipital extending from occipital condyle to basal tuber; so, supraoccipital; vic, videan canal; XII, foramina for cranial nerve XII.

51.6219° N, 2.4299° W). Late Triassic fissure fill deposits of either Carnian–Norian (Simms, 1990; Simms & Drost, 2022; Walkden et al., 2021; Walkden & Fraser, 1993) or Rhaetian (Morton et al., 2017; Whiteside et al., 2016; Whiteside & Marshall, 2008) age. AUP 11308 was collected from Site 1, Cromhall Quarry.

Etymology: The genus name is derived from *Hwicce* (pronounced “hwit-chuh”), a tribal kingdom of Anglo-Saxon England covering parts of modern-day Gloucestershire, Worcestershire and Warwickshire, including the type site, and the Old English *wurm*, meaning dragon. The species name is from the Latin *tri*, meaning three, and *spiculum*, meaning spear, and refers to the diagnostic three projections on the quadratojugal.

Comments: Fraser (1986:Figure 6) briefly mentioned and illustrated procolophonid material from Cromhall

Quarry found at site 5A (Walkden & Fraser, 1993) with tricuspid maxillary crowns with a subtriangular outline in occlusal view. Edwards (2000) referred to this material as “procolophonid a”, noted that it was characterized by three maxillary teeth and four dentary teeth with highly differentiated upper and lower dentitions, and suggested that it is a distinct species to the material described here from site 1, which was referred to as “procolophonid b”. Edwards (2000) also suggested that specimens identified by Halstead and Nicoll (1971: plate 24) as procolophonid and trilophosaurid actually belong to “procolophonid a”. Further consideration of the material referred to as “procolophonid a” will be provided elsewhere.

4 | DESCRIPTION

The holotype and referred material of *H. trispiculum* comprise a range of cranial and postcranial elements.

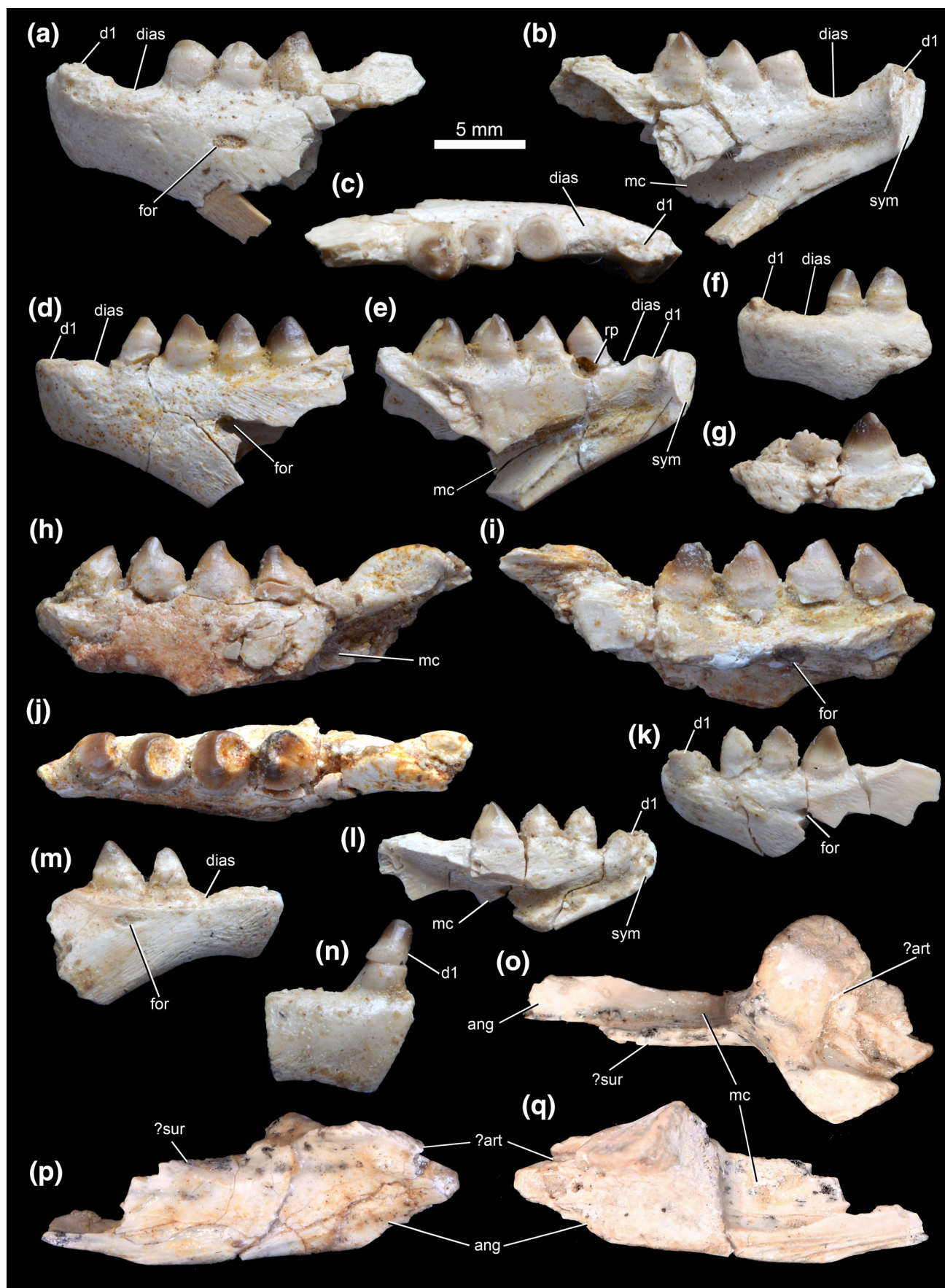


FIGURE 8 Legend on next page.

Nearly all material is disarticulated, except for a few cranial specimens that are preserved in articulation (e.g., the holotype: Figures 2, 3). Although there is no information recorded on how the specimens were originally discovered and grouped together, preservation style is consistent throughout the material described here, and all morphology is consistent with that of a leptopleuronine procolophonid. Surface bone preservation is generally good, not heavily fractured, and with good anatomical detail visible. Specimens are preserved in three dimensions with minimal evidence of crushing or shearing. The number of individuals represented is uncertain, but the minimum estimate for the UMZC material is six based on the number of left dentaries. There are a range of sizes present, which could reflect different ontogenetic stages, sexual dimorphism or other intraspecific variation.

4.1 | Premaxilla

There are four specimens which include the premaxilla. The element is best preserved in the holotype (UMZC 2023.4.1; Figures 2, 3), which includes the entire left premaxilla and fragments of the right. UMZC 2023.4.2 preserves a complete right premaxilla in articulation with the right maxilla (Figure 4i–k). UMZC 2023.4.3 is an isolated left premaxilla (Figure 4a, b, e). Fragments of a right premaxilla are preserved in articulation with the incomplete right maxilla of UMZC 2023.4.4 (Figure 4c, d, h).

The premaxilla forms most of the anterior, ventral and posterior borders of the external naris. The external naris is oval, with the long axis extending from anteroventral to posterodorsal. The anterior border of the external naris is positioned directly above the first premaxillary tooth (Figures 2a, 4j), similar to the condition in *Hypsognathus*, *Leptopleuron* and *Soturnia* (Cisneros & Schultz, 2003; Säilä, 2010; Sues et al., 2000), but differing from the condition seen in most procolophonids, where the anterior border of the naris is located anterior to the premaxillary teeth (Cisneros, 2008; Säilä, 2010).

The premaxilla has a rectangular main body, forming the ventral border of the naris, from which two processes arise. The prenarial process is directed anterodorsally,

such that the anteriormost tip of the snout projects slightly anterior to the anteriormost tooth (Figure 4j), and forms most of the anterior margin of the naris and, together with its antimeres, the internarial bar (Figure 2e). The internarial bar is not as broad as that of *Hypsognathus* (Sues et al., 2000: Figure 2d), and more similar to that of *Leptopleuron* (Säilä, 2010). The postnarial process is generally poorly preserved with fracturing of the bone surface in all specimens in which it is present. It forms a contact with the nasal at a point level with the posterodorsal corner of the external naris, excluding the maxilla from the boundary of the latter. UMZC 2023.4.3 is missing most of the pre- and postnarial processes, but above the second premaxillary tooth the lateral surface is striated for contact with the maxilla (Figure 4a), indicating that the latter overlapped the premaxilla laterally.

Most of the premaxillary palate is broken in the available specimens, but a large, oval foramen (“foramen prepalatinum”) is visible in UMZC 2023.4.1, UMZC 2023.4.2 and UMZC 2023.4.3 (Figures 2c, 4e, k, fpp), medial to the second premaxillary tooth, as in the leptopleuronines *Leptopleuron*, *Hypsognathus* and *Soturnia* (Cisneros & Schultz, 2003; Säilä, 2010; Sues et al., 2000) but differing from the condition in other procolophonids. The contact with the vomer is unknown. It is unclear if a separate septomaxilla was present or not. The septomaxilla appears to be absent in *Leptopleuron* and *Hypsognathus* (Säilä, 2010; Sues et al., 2000) but is present in at least some other procolophonids (e.g., *Procolophon*, Carroll & Lindsay, 1985).

Premaxillary teeth are preserved in UMZC 2023.4.1, UMZC 2023.4.2, and UMZC 2023.4.3 (Figures 2, 4). There are two teeth, as in most leptopleuronines (Cisneros, 2008; Cisneros & Schultz, 2003; Säilä, 2010; Sues et al., 2000; Tsuji, 2018). These teeth are monocuspid and incisiform, lacking the labiolingual expansion seen in the maxillary teeth, and are similar in apicobasal height to the middle maxillary teeth. In UCMZ 2023.4.2 the premaxillary teeth are similar in size to one another (Figure 4i–k). However, in UCMZ 2023.4.3, the first tooth is substantially larger than the second (Figure 4a, b, e), as in many other procolophonids including *Scoloparia*, *Hypsognathus*, *Soturnia* and *Leptopleuron* (Cisneros, 2008; Cisneros & Schultz, 2003;

FIGURE 8 *Hwiccewyrn trispiculum* gen et sp. nov., dentaries, referred specimens. (a–c) UMZC 2023.4.20, partial left dentary in lateral (a), medial (b) and dorsal (c) views. (d, e) UMZC 2023.4.21, partial left dentary in lateral (d) and medial (e) views. (f) UMZC 2023.4.23, fragment of anterior left dentary in lateral view. (g) UMZC 2023.4.24, fragment of left dentary in lateral view. (h–j) UMZC 2023.4.19, partial left dentary in lateral (h), medial (i) and dorsal (j) views. (k, l) UMZC 2023.4.22, partial left dentary in lateral (k) and medial (l) views. (m) UMZC 2023.4.25, partial right dentary in lateral view. (n), UMZC 2023.4.26, partial right dentary in lateral view. (o, p, q) UMZC 2023.4.29, posterior section of left mandible in dorsal (o), lateral (p), and medial (q) views. ang, angular; art, articular; d1, procumbent first dentary tooth; dias, diastema between first and second dentary teeth; for, foramen on lateral surface of dentary; mc, Meckelian canal; rp, resorption pit; sur, surangular; sym, mandibular symphysis.

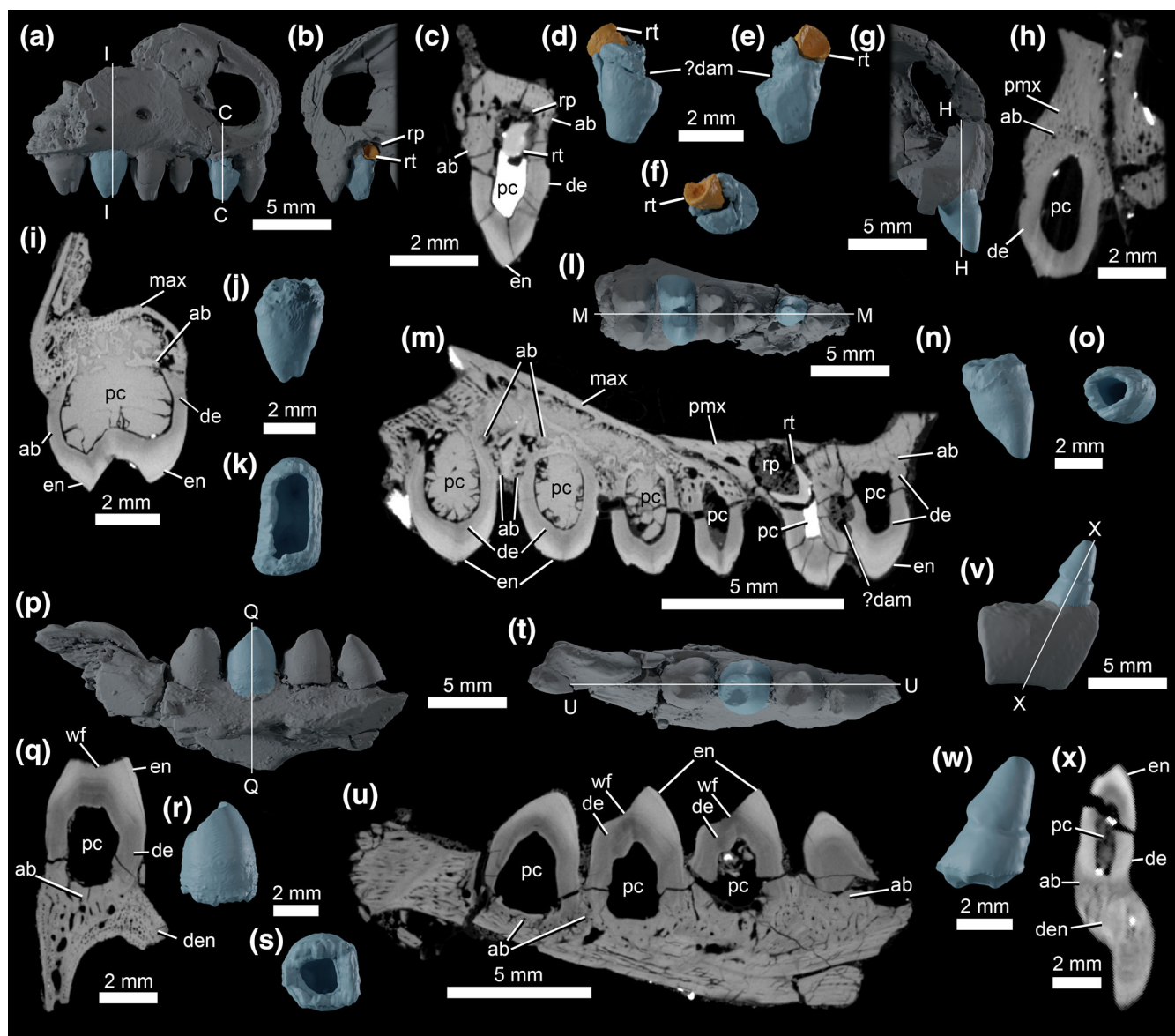


FIGURE 9 *Hwiccewurm trispiculum* gen et sp. nov., details of tooth implantation and replacement. (a, b) UMZC 2023.4.2, partial right premaxilla, maxilla and nasal in lateral view (a), showing location of cross sections shown in figure parts (c) and (i), and medial view (b). (c) Coronal cross section through UMZC 2023.4.2 second premaxillary tooth, replacement tooth and resorption pit. (d–f), segmentation of UMZC 2023.4.2 second premaxillary tooth and replacement tooth in lateral (d), medial (e), and dorsal (f) views. (g) Anterior of UMZC 2023.4.1 in medial view showing location of cross section (h). (h) Coronal cross section through UMZC 2023.4.1 first premaxillary tooth. i, coronal cross section through UMZC 2023.4.2 third maxillary tooth. (j, k) Segmentation of UMZC 2023.4.2 third maxillary tooth in lateral (j) and dorsal (k) views. (l) Ventral view of UMZC 2023.4.2 showing location of cross section (m). (m) Sagittal cross section through premaxillary and maxillary teeth of UMZC 2023.4.2 showing ongoing replacement of second premaxillary tooth. (n, o) Segmentation of UMZC 2023.4.1 first premaxillary tooth in lateral (n) and dorsal (o) views. (p) Partial left dentary UMZC 2023.4.19 in medial view showing location of cross section (q). (q) Coronal cross section through UMZC 2023.4.19 fourth dentary tooth. (r, s) Segmentation of UMZC 2023.4.19 fourth dentary tooth in medial (r) and ventral (s) views. (t) Dorsal view of UMZC 2023.4.19 showing location of cross section (u). (u) Sagittal cross section through dentary teeth of UMZC 2023.4.19. (v) Lateral view of partial right dentary UMZC 2023.4.26 and procumbent first dentary tooth showing location of cross section (x). (w) Segmentation of UMZC 2023.4.26 procumbent first dentary tooth in lateral view. (x) Oblique cross section through UMZC 2023.4.26 procumbent first dentary tooth. ab, attachment bone; dam, damage; de, dentine; en, enamel; max, maxilla; pc, pulp cavity; pmx, premaxilla; rp, resorption pit; rt, replacement tooth; wf, wear facet.

Säilä, 2010; Sues et al., 2000; Sues & Baird, 1998). Only the first premaxillary tooth is preserved in the holotype (UMZC 2023.4.1; Figure 2). In this specimen the first premaxillary tooth is procumbent, but in UMZC 2023.4.2 (Figure 4i–k)

and UMZC 2023.4.2 (Figure 4a, b) the first premaxillary tooth is directed ventrally. The teeth are indistinguishably fused at their bases to the surrounding bone – details of tooth implantation are described below. The first

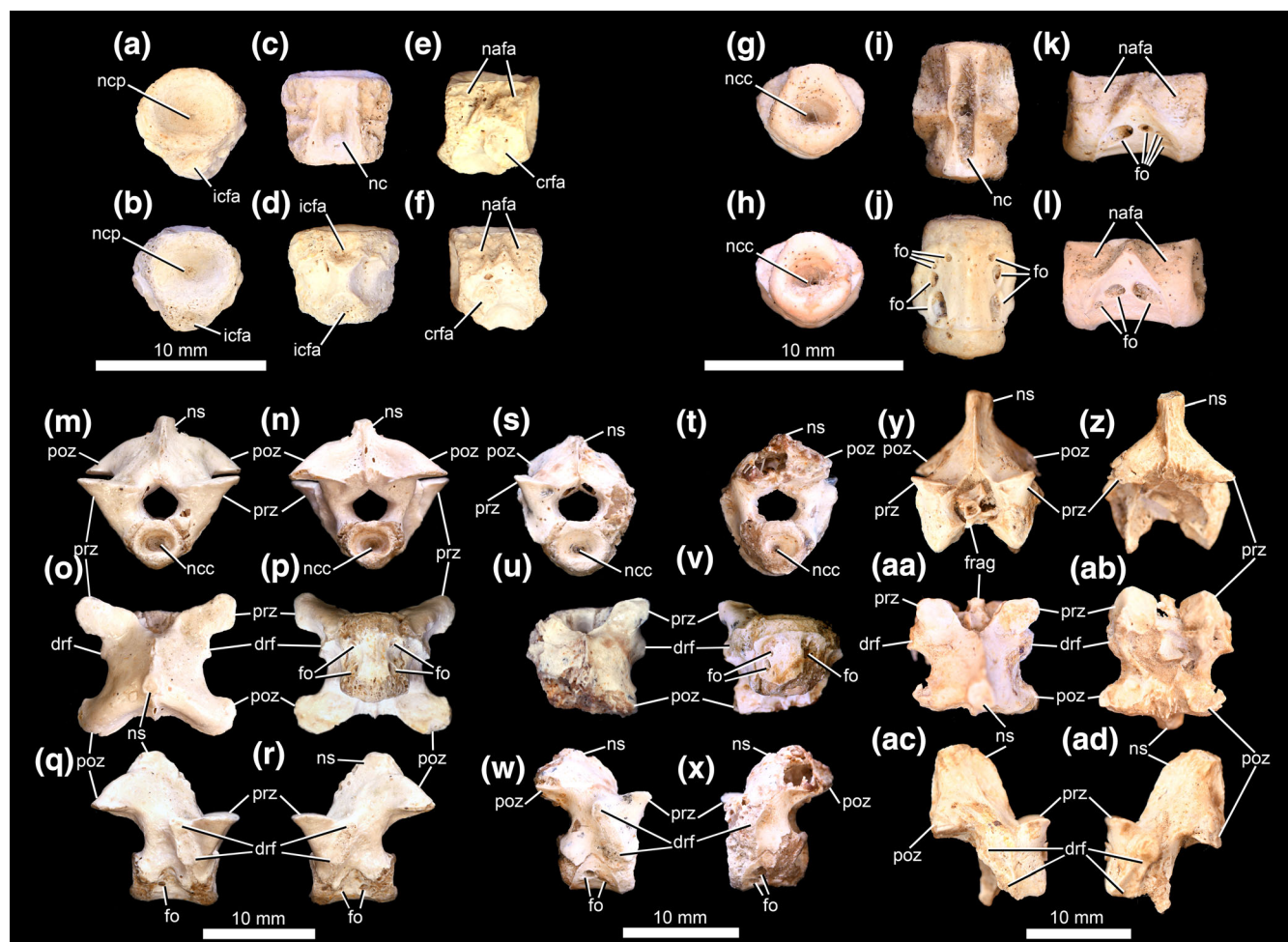


FIGURE 10 *Hwiccewyrms trispiculum* gen et sp. nov., vertebral material, referred specimens. (a–f) UMZC 2023.4.30, cervical centrum in anterior (a), posterior (b), dorsal (c), ventral (d), right lateral (e), and left lateral (f) views. (g–l), UMZC 2023.4.34, dorsal centrum in anterior (g), posterior (h), dorsal (i), ventral (j), right lateral (k), and left lateral (l) views. (m–r), UMZC 2023.4.31, complete dorsal vertebra in anterior (m), posterior (n), dorsal (o), ventral (p), right lateral (q) and left lateral (r) views. (s–x) UMZC 2023.4.32, complete dorsal vertebra in anterior (s), posterior (t), dorsal (u), ventral (v), right lateral (w) and left lateral (x) views. (y–AD), UMZC 2023.4.33, dorsal neural arch in anterior (y), posterior (z), dorsal (AA), ventral (AB), right lateral (AC), and left lateral (AD) views. crfa, facet for the cervical rib; drf, facet for dorsal rib; fo, foramina; frag, fragment of another bone in neural canal; icfa, facet for the intercentrum; nafa, facet for the neural arch; nc, neural canal; ncc, notochordal canal; ncp, notochordal pit; ns, neural spine; poz, postzygapophysis; prz, prezygapophysis.

premaxillary tooth of UMZC 2023.4.1 and UMZC 2023.4.3 bears an elongate, high-angle wear surface on its distal surface (Figures 2b, 4b). A similar wear facet in *Scoloparia* was proposed to have formed during contact with the procumbent anterior tooth of the dentary (Sues & Baird, 1998). In UMZC 2023.4.3, the second premaxillary tooth has a low-angle wear facet on the lingual surface of its apex (Figure 4b).

4.2 | Maxilla

There are six maxillae (Figures 2–4), three from the left side (UMZC 2023.4.1, UMZC 2023.4.5, UMZC 2023.4.6) and three from the right (UMZC 2023.4.2, UMZC

2023.4.4, UMZC 2023.4.7). The best-preserved example is the left maxilla of the holotype (UMZC 2023.4.1; Figures 2, 3). In lateral view, the maxilla is almost as tall dorsoventrally as it is long anteroposteriorly. There is no maxillary fossa posterior to the external naris, unlike the condition in many procolophonids, but similar to the condition in *Scoloparia*, *Leptopleuron*, *Soturnia* and *Hypsognathus* (Cisneros, 2008; Säilä, 2010; Sues et al., 2000; Sues & Baird, 1998). The maxilla laterally overlaps the premaxilla anteriorly (see above). Dorsally it has an anteroposteriorly extending suture with the nasal, and although the jugal is not preserved in articulation there is an extensive sutural surface for this element posteriorly (Figure 2a, ajg). Medially, the maxilla is transversely expanded along its posterior

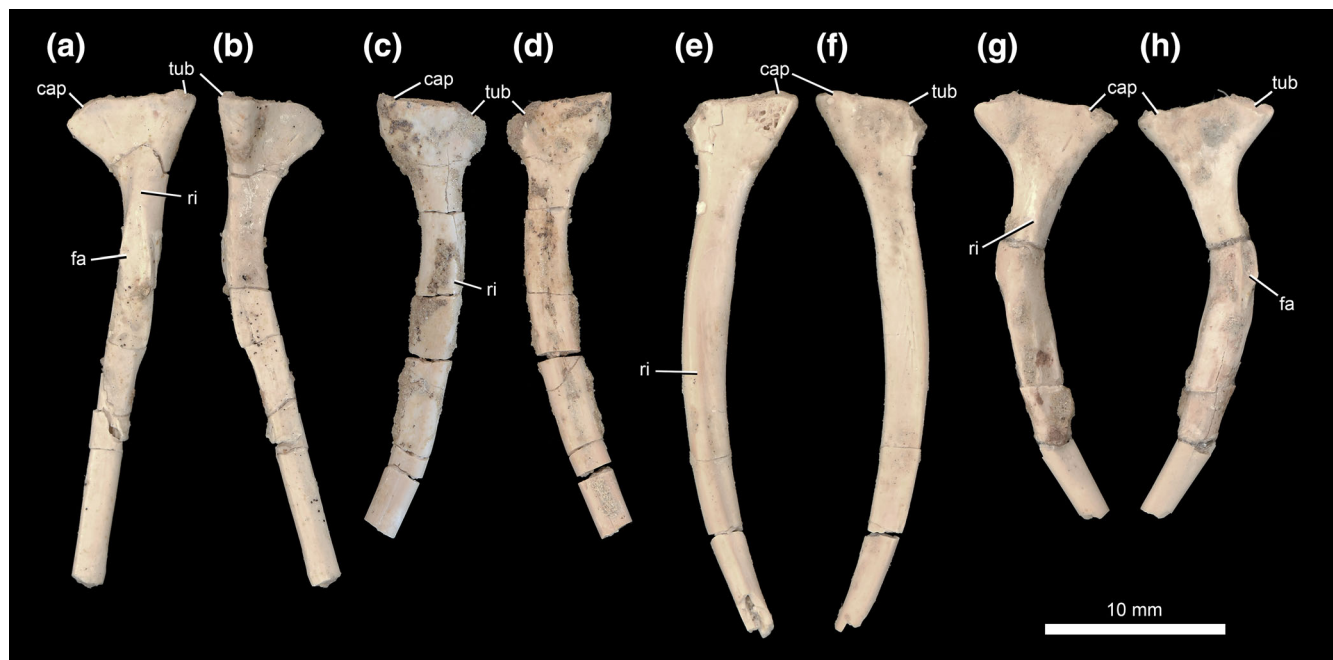


FIGURE 11 *Hwiccewyrms trispiculum* gen et sp. nov., ribs, referred specimens. (a, b) UMZC 2023.4.35, left rib in anterior (a) and posterior (b) views. (c, d), UMZC 2023.4.36, left rib in anterior (c) and posterior (d) views. (e, f), UMZC 2023.4.37, right rib in anterior (e) and posterior (f) views. (g, h), UMZC 2023.4.38, left rib in anterior (g) and posterior (h) views. cap, capitulum; fa, facet on anterior surface; ri, ridge on anterior surface, tub, tubercle.

half to form the articulation with the ectopterygoid (Figure 2d, f).

There are two supralabial foramina on the lateral surface of the maxilla (Figure 2a). The first of these is larger and is positioned above the second maxillary tooth at about mid-height of the element (Figures 2a, 4c, f, g, j, mfo1). The second is close to, or on the margin of, the sutural surface for the jugal, above the third maxillary tooth or the gap between the third and fourth teeth (Figure 2a, 4c, j, mfo2). Two supralabial foramina, with the more anterior being larger, are also present in similar positions in *Hypsognathus* and *Leptopleuron* (Säilä, 2010; Sues et al., 2000), although the more posterior foramen is more broadly separated from the jugal in these species.

A short diastema, with a length less than the mesiodistal width of a single crown, separates the premaxillary and maxillary tooth rows (Figure 2c). There are four maxillary teeth, differing from the condition in *Leptopleuron* (five teeth; Säilä, 2010), *Mandaphon* (six teeth; Tsuji, 2018) and *Scoloparia* (six teeth; Sues & Baird, 1998), but more similar to *Hypsognathus* (four or five teeth; Sues et al., 2000). This tooth count appears to be consistent in all specimens in which it can be assessed, regardless of size (Figures 2, 4h, k). The teeth are indistinguishably fused at their bases to the surrounding bone—tooth implantation is described below. All maxillary teeth are molariform, with transversely

expanded bases and crowns and mesiodistally broad bases (Figures 2–4). This is similar to the condition in *Leptopleuron*, *Soturnia* and *Scoloparia* (Cisneros, 2008); by contrast, in *Hypsognathus* the first maxillary tooth is conical (Sues et al., 2000). The teeth have a well-developed lingual cusp whereas labially what appears at first impression as a single labial cusp is actually subtly subdivided in maxillary teeth 2–4 into two cusps, differentiated from one another in part by a shallow, apicobasally extending groove on the lingual surface (Figure 2b). Maxillary crowns 2–4 are therefore tricuspid, with a lingual cusp and two subtly subdivided labial cusps, but wear facets tend to obliterate the subdivision between the two labial cusps making the crowns appear bicuspid. The first maxillary tooth is not as expanded labiolingually as the more posterior teeth and appears to be bicuspid rather than tricuspid. In smaller specimens (UMZC 2023.4.2; Figure 4k) the first maxillary tooth is not much more expanded transversely than the premaxillary teeth but is still bicuspid. In larger specimens (UMZC 2023.4.1; Figure 2g) the first maxillary tooth is much more expanded transversely, and this variation is likely ontogenetic. In lateral view, the first tooth is also shorter apicobasally than maxillary teeth 2–4, which are subequal in size (Figures 2a, 4c, j). There are deep occlusal depressions between the labially and lingually positioned cusps in maxillary teeth 2–4 (Figure 2g), as in

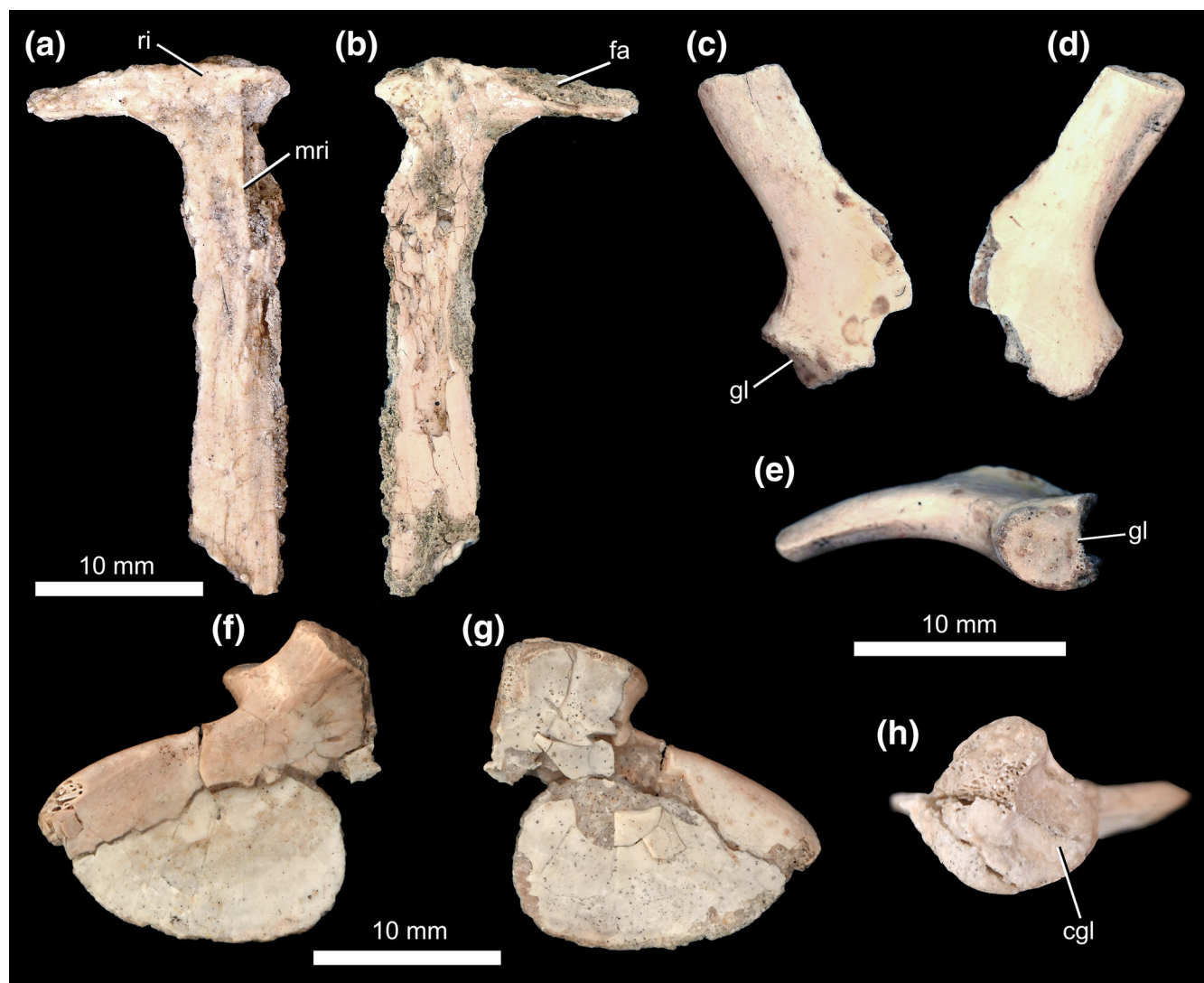


FIGURE 12 *Hwiccewyrms trispiculum* gen et sp. nov., pectoral girdle elements, referred specimens. (a, b) UMZC 2023.4.39, partial interclavicle in ventral (a) and dorsal (b) views. (c–e) UMZC 2023.4.40, right scapula in lateral (c), medial (d) and ventral (e) views. (f–h) UMZC 2023.4.41, left metacoracoid in ventral (f), dorsal (g), and proximal views (h). cgl, contribution of metacoracoid to glenoid fossa; fa, anterior facet for the clavicle; gl, glenoid fossa on scapula; mri, median ridge running along median process of interclavicle; ri, raised ridge on anteroventral margin of lateral process of interclavicle.

Soturnia and *Hypsognathus* (Cisneros, 2008). Wear facets are best preserved in the holotype (Figure 2c, g).

4.3 | Nasal

The nasals are partially preserved in UMZC 2023.4.1, UMZC 2023.4.2 and UMZC 2023.4.4 (Figures 2, 3, 4c, d, i, j), and the bone has anterior and anteroventral processes that frame the dorsal, anterodorsal, and posterodorsal margins of the external naris. Some fragments of prefrontal and/or lacrimal are probably preserved in UMZC 2023.4.1 but are too badly damaged to provide detail on the nature of their contacts with the nasal.

There is a foramen on the lateral surface of the nasal, just above the posterodorsal corner of the naris (Figures 2a, 4c, j, nfo5). This foramen opens anteriorly, and in UMZC UMZC 2023.4.1 has a shallow groove extending anteriorly from it. On the medial surface of the nasal, there is a foramen just above the posterodorsal corner of the external naris that may connect to the aforementioned lateral foramen (Figures 2b, 4i, mnfo). A groove extends posterodorsally away from this medial foramen (UMZC 2023.4.2; Figure 4i, ngr). On the lateral surface of the nasal there is a cluster of three foramina in a triangular arrangement just posterior to the first lateral foramen (Figures 2a, 4j, nfo2–4). There are three corresponding foramina on the medial surface (best preserved in UMZC 2023.4.1; Figure 2b, c).



FIGURE 13 *Hwiccewyrms trispiculum* gen et sp. nov., forelimb elements, referred specimens. (a–f) UMZC 2023.4.42, left humerus in posteroventral (a), posterior (b), anterodorsal (c), anterior (d), proximal (e), and distal (f) views. (g–l), UMZC 2023.4.43, left humerus in posteroventral (g), posterior (h), anterodorsal (i), anterior (j), proximal (k) and distal (l) views. (m–r) UMZC 2023.4.45, left radius in anterior (m), medial (n), posterior (o), lateral (p), proximal (q) and distal (r) views. ?cap, capitulum; dpc, deltopectoral crest; ect, ectepicondyle; ent, entepicondyle; entf, entepicondylar foramen; fo, foramen; ?tr, trochlea.

Another foramen is present at the contact between the anteroventral process of the nasal and the postnarial process of the premaxilla, visible on both lateral and medial surfaces (Figures 2a, d, e, 4c, j, nfo1).

4.4 | Frontal

A single left frontal is preserved in the UMZC material (UMZC 2023.4.8; Figure 5a, b). The frontal is very flat,

with a slight dorsoventral thickening laterally where it forms the anterodorsal portion of the margin of the orbitotemporal fenestra. The bone is dorsoventrally thickened at its anterolateral corner where it would have contacted either the lacrimal or prefrontal (Figure 5b; these bones are unknown in *Hwiccewyrms* and their size and orientation are variable in other leptopleuronines: Sues et al., 2000; Säilä, 2010). The anterior end of the bone is broken, so the anterior extent of the frontal and the nature of the contact with the nasal are unknown.

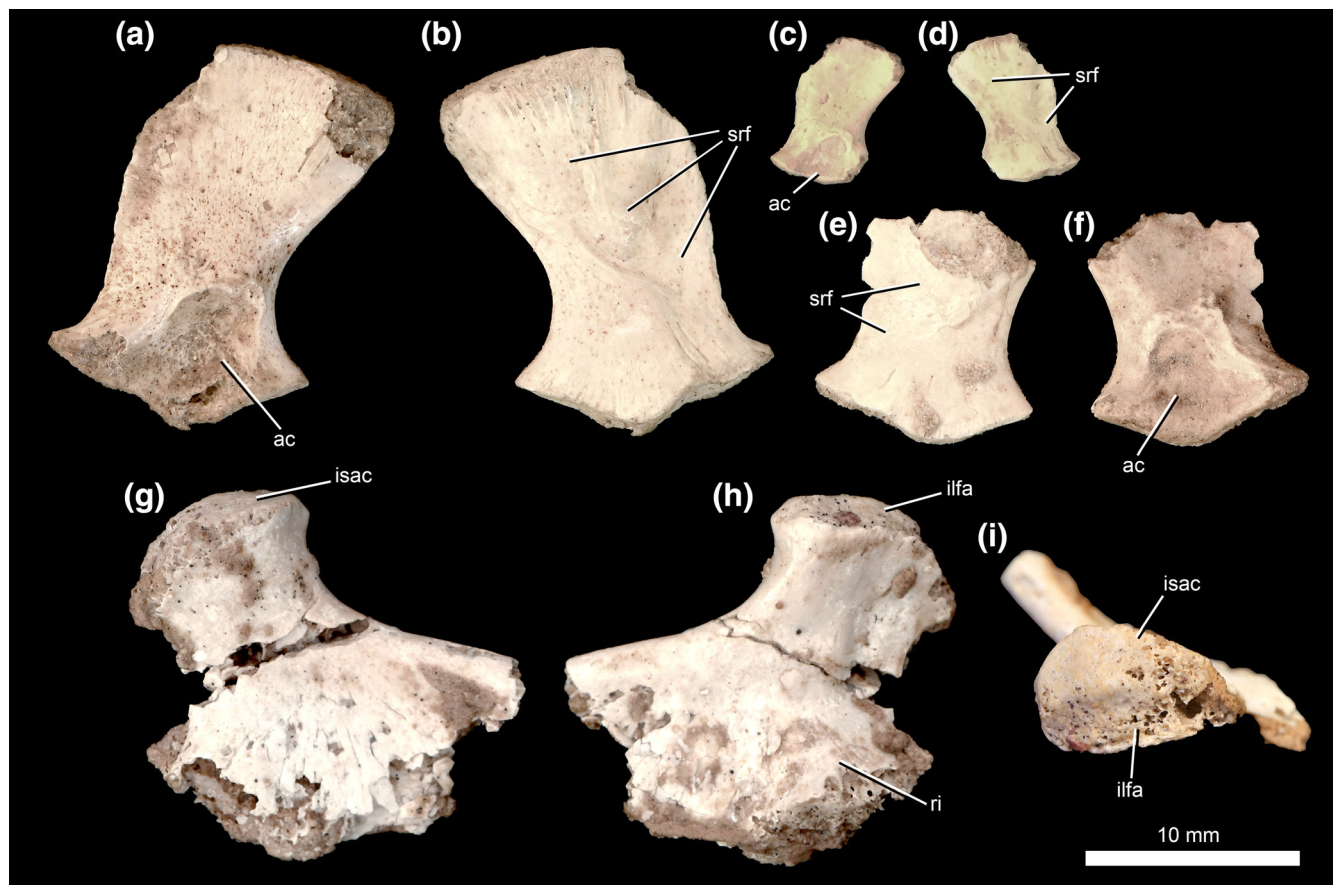


FIGURE 14 *Hwiccewyrms trispiculum* gen et sp. nov., pelvic elements, referred specimens. UMZC 2023.4.46, left ilium in lateral (a) and medial (b) views. UMZC 2023.4.47, left ilium in lateral (c) and medial (d) views. UMZC 2023.4.48, right ilium in medial (e) and lateral (f) views. UMZC 2023.4.49, left ischium in lateral (g), medial (h) and proximal (i) views. ac, acetabulum; ilfa, facet on the ischium for articulation with the ilium; isac, ischial contribution to the acetabulum; ri, low ridge on dorsal surface of the ischium blade; srf, depressed area on medial surface of ilium for articulation of the sacral ribs.

The medial suture with the opposing frontal was antero-posteriorly straight. The posterior sutural surface for the parietal shows some damage but appears to have been primarily a straight transverse contact (Figure 5a, b). A pair of frontals from the Aberdeen collection (AUP 11308) show essentially the same morphology as UMZC 2023.4.8 (Figure 6) and are therefore also referred to *Hwiccewyrms* here.

4.5 | Parietal

There are two specimens that include parts of the parietal. UMZC 2023.4.9 is articulated partial left and right parietals (Figure 5c, g), preserving part of the rim of the left orbitotemporal fenestra and the left posterolateral rim of the pineal foramen. UMZC 2023.4.10 is the posterior portion of an incomplete right parietal (Figure 5d). The parietal is dorsoventrally flattened like the frontal, and the dorsal surface is flat but slightly thickened at the

orbitotemporal margin (Figure 5c, orbr), as in the frontal, and also close to the posteriormost portion of the bone, where it forms a low transverse ridge (Figure 5c, occr). While the full extent of this ridge is not preserved, the shape of what is present suggests that the ridge formed a posteriorly projecting point at the midline, as in *Leptopleuron* (Säilä, 2010). Posterior to this ridge, there is a posteroventrally directed ledge that is best developed medially and would have overhung the occiput (Figure 5c, occlg; the occipital ledge of Säilä, 2010). At the posterolateral corner of the parietal there is a sutural surface preserved for the supratemporal (Figure 5d, ast; Säilä, 2010). The preserved margin of the pineal foramen (Figure 5c, g, pif) suggests that this opening was relatively large. Its posterior margin was located a short distance anterior to the posterior margin of the orbitotemporal fenestra, similar to the condition in *Leptopleuron* (Säilä, 2010) but differing from the condition in *Hypsognathus* in which the pineal foramen is positioned far anteriorly (Sues et al., 2000).



FIGURE 15 *Hwiccewyrms trispiculum* gen et sp. nov., hindlimb elements, referred specimens. UMZC 2023.4.50, left femur in ventral (a), posterior (b), dorsal (c), anterior (d), proximal (e) and distal (f) views. UMZC 2023.4.51, right femur in ventral (g), posterior (h), dorsal (i), anterior (j), proximal (k), and distal (l) views. ar, adductor ridge; icf, intercondylar fossa; it, internal trochanter; itf, intertrochanteric fossa; ps, popliteal space.

4.6 | Supratemporal

Partial left (UMZC 2023.4.11; Figure 5l, o, p) and right (UMZC 2023.4.12; Figure 5m, n, q) supratemporals are preserved and are of similar size to one another. The dorsal surface of the supratemporal is flat and broad and formed the strongly projecting posterolateral corner of the skull and the posterolateral border of the orbitotemporal opening (Figure 5l, m, orb), similar to the

condition in *Hypsognathus* (Sues et al., 2000) but differing from the condition reconstructed for *Leptopleuron* in which the supratemporal is shown as excluded from the boundary of the orbitotemporal fenestra and formed a smaller area of the posterior skull roof (Säilä, 2010). The supratemporal has a posteroventrally sloping shelf that was continuous with the occipital ledge of the parietal. Anteriorly, two sutural surfaces, which may have been for the quadratojugal and jugal (based on

comparison to *Hypsognathus*; Sues et al., 2000), are preserved (Figure 5l, m, ?ajg, ?aqj). On the ventral surface there is a well-developed, anteroposteriorly extending ridge, on which a small foramen is positioned at mid-length (Figure 5n, o, ri, for).

4.7 | Quadratojugal

There are four examples of the quadratojugal, three of which appear to be from the left side (UMZC 2023.4.13, Figure 5h, i; UMZC 2023.4.14; UMZC 2023.4.15, Figure 5j, l) and one from the right (UMZC 2023.4.16). They show considerable variation in size, from the smallest (UMZC 2023.4.15) to the largest (UMZC 2023.4.14). None of them is completely preserved, but UMZC 2023.4.13 is the most complete and is in articulation with a partial left jugal. The quadratojugal bears two large spines towards the posteroventral margin of the bone, which are approximately equal in size in UMZC 2023.4.13 (Figure 5h). In UMZC 2023.4.15, however, the anterior spine is longer than the posterior one (Figure 5j, l). The robustness of the spines appears to increase in larger specimens. Säilä (2010) described the spines of *Leptopleuron* as dorsoventrally flattened. In *Hwiccewyrn* the condition for this character is variable, with some being dorsoventrally compressed and others conical with limited dorsoventral compression. The more anterior spine points ventrolaterally while the posterior spine is posterolaterally directed. The surfaces of the spines are pitted, with grooves extending from the base towards the apex in UMZC 2023.4.14; these pits likely reflect an overlying keratinous sheath. The spines are each set in a shallow crater surrounded by a raised rim of bone. The external surface of the quadratojugal has grooves and a rugose surface texture similar to that described by Säilä (2010) for *Leptopleuron* (Figure 5h).

The quadratojugal laterally overlaps the jugal anterodorsally. There is a broad and gently concave area on the lateral surface that separates the spines from this contact (Figure 5h). At the anterior margin of this surface there is a small, raised boss (Figure 5h). A similar boss on the anterior margin of the quadratojugal has not been reported in other leptopleuronines. Although quite distinct in morphology from the two spines, this feature was referred to as a “third small quadratojugal spine” by Fraser (1994) and suggested as a distinct feature of the Cromhall specimens (see also Edwards, 2000). On the medial surface of the bone there is a posteriorly placed articular facet that extends from posteroventral to anterodorsal for the body of the quadrate. Part of the quadrate is preserved in articulation with this facet in UMZC 2023.4.13.

4.8 | Quadrate

A small fragment of the shaft of the right quadrate shaft is present in articulation with the quadratojugal in UMZC 2023.4.13 but does not provide useful anatomical information (Figure 5i).

4.9 | Jugal

UMZC 2023.4.17 is a right jugal missing the anteriormost portion and with some damage to its ventral margin (Figure 5e, f). The posterior part of a left jugal is preserved in articulation with the quadratojugal in UMZC 2023.4.13 (Figure 5h, i). The jugal formed the ventral margin of the orbitotemporal fenestra. This margin is concave, and similar in its curvature to *Leptopleuron* (Säilä, 2010). The lateral surface of the posterior end of the jugal is depressed and striated where it was laterally overlapped by the quadratojugal (Figure 5e). The postero-dorsal corner of the element is drawn out into a postorbital process which is striated medially where it would have overlapped the postorbital (Figure 5i). At the anterior end, damage to the bone makes it difficult to assess the nature of the contacts with the maxilla and ectopterygoid. An internal canal is visible at the anterior end due to this breakage, but it is uncertain where this canal emerges on the bone surface. There is no groove on the lateral surface of the bone, differing from the condition in *Leptopleuron* (Säilä, 2010). The jugal is much shallower dorsoventrally than that of *Hypsognathus* (Sues et al., 2000) and lacks a ridge or tubercle on the lateral surface.

4.10 | Palatine

Part of the left palatine is preserved in UMZC 2023.4.1 (Figures 2, 3). It is anteroposteriorly short in ventral view, contacting the maxilla medial to the most posterior tooth and the ectopterygoid posteriorly. It has a dorsal process (Figure 2d, f, dppal) that is overlapped anterolaterally by a narrow process of the maxilla and that contacts the ectopterygoid posteroventrally. No teeth are present on the palatine.

4.11 | Ectopterygoid

A complete left ectopterygoid is preserved in articulation with the posterior portion of the maxilla in UMZC 2023.4.1 (Figures 2, 3). It is vertically oriented and dorsally forks into two processes. The first process is laterally

directed, articulates with the posterior end of the maxilla, and terminates in a concave facet for articulation with the jugal. The second process is short and anterodorsally directed and articulates with the palatine. There is a concave facet on the medial surface of the ectopterygoid for the articulation of the pterygoid (Figures 2b, 3b, aptg), and this facet extends to the ventral margin of the bone. The main body of the ectopterygoid, which formed the transverse flange together with the pterygoid, is dorsoventrally tall and transversely compressed.

4.12 | Braincase

UMZC 2023.4.18 is an articulated partial braincase (Figure 7), comprising a basisphenoid lacking the anterior portion including the basiptyergoid processes, most of the basioccipital, a nearly complete left exoccipital, and the supraoccipital.

As in *Leptopleuron* (Spencer, 2000) the basioccipital has a long anterior portion that forms much of the internal floor of the braincase, with lateral margins that are flattened, face dorsolaterally, and which form the ventral margin of the fenestra ovalis (Figure 7b, c). On the dorsal surface of this anterior extension of the basioccipital there is a narrow midline crest that extends anteriorly. This crest is most prominent close to the foramen magnum and becomes less prominent anteriorly. There are foramina present on the floor of the braincase either side of this crest, including two particularly prominent paired foramina just medial to the posterior margin of the fenestra ovalis. The anteriormost end of the basioccipital does not appear to be bilobed where it contacts the basisphenoid, unlike the condition described for *Leptopleuron* (Spencer, 2000).

On the occiput the basioccipital forms the majority of the occipital condyle (Figure 7a). The dorsolateral corners of the basioccipital are excavated to articulate with the exoccipitals, which can be inferred to have approached each other closely on the midline, largely excluding the basioccipital from the ventral margin of the foramen magnum. The occipital condyle is tripartite as in *Leptopleuron* and *Hypsognathus* (Cisneros, 2008), with clear sutures between the basioccipital and exoccipitals, and the overall structure of the condyle is very similar to that of *Leptopleuron* (Spencer, 2000). The condyle is reniform and has a concave posterior surface. There is a small indentation on the midline that may be the notochordal pit as in *Leptopleuron* (Spencer, 2000).

The basal tubera are relatively small (Figure 7a, e). They sit at the end of short ventrolaterally extending processes that have low ridges on the posterior surfaces (Figure 7a, ri). The tubera are separated from one another by a deep central notch. A triangular anterior

projection of the basioccipital is present on the midline (Figure 7e, apbo), between the basal tubera, and forming the roof of a deep funnel-shaped concavity that is confluent with the basisphenoid fossa. The basal tubera of the basioccipital project ventrolaterally and each is sheathed ventrally by a thin posterior process of the basisphenoid (Figure 7e, ppbs), although this process has broken away on the right side and is damaged on the left. The suture between the basioccipital and the basisphenoid is not clearly visible on the lateral surface, but the lateral surface is strongly concave dorsoventrally, particularly above the basal tubera.

Only the left exoccipital is preserved in UMZC 2023.4.18 (Figure 7a, b, e). As mentioned above, the exoccipitals can be inferred to have approached each other closely on the midline at their posterior ends and formed the dorsolateral components of the occipital condyle. The dorsolateral corner of the exoccipital is expanded to form a sutural surface for the opisthotic (Figure 7b, f, aop). This surface is subquadrangular and slightly concave, and faces anterodorsally, and contrasts with the description of the same contact as “dome-like” in *Leptopleuron* (Spencer, 2000). The supraoccipital is preserved in articulation with the exoccipital dorsomedially, but it is not possible to describe the exact nature of this contact as the bone is heavily fractured in this area.

There is no strong anteroventrally directed ridge on the lateral surface of the exoccipital, contrasting with that described for *Leptopleuron* (Spencer, 2000). There are three foramina on the lateral surface (Figure 7b), arranged in an anteroposteriorly oriented line, presumably for cranial nerve XII (hypoglossal) as in *Leptopleuron* (Spencer, 2000:Figure 7). The anterior part of the exoccipital thins transversely, becoming very narrow transversely anteriorly where it forms the posterior border of the fenestra ovalis. There is no longitudinal groove on the dorsal surface of the anterior end of the exoccipital, unlike the condition in *Leptopleuron* (Spencer, 2000). The medial surface of the exoccipital is concave dorsoventrally and anteroposteriorly, three foramina for cranial nerve XII are clearly visible (Figure 7d), corresponding to those visible on the lateral surface of the bone.

The supraoccipital is arch shaped and comprises the majority of the dorsal border of the foramen magnum (Figure 7a). There is a short ascending process extending anterodorsally that presumably articulated with the parietals. The supraoccipital articulates with the exoccipital posterolaterally, but this area is damaged so the exact nature of the suture is hard to determine. Due to damage to the margins of the bone, the sutural surfaces for the opisthotics and prootics are not preserved.

The elongate basisphenoid is incompletely preserved (Figure 7b, d, e), missing the basiptyergoid processes and basisphenoid rostrum. Its contacts with the basioccipital cannot be fully determined laterally, although it underlies the anterior extension of the basioccipital, and ventrally thin posterior processes of the basisphenoid sheath the basal tubera of the basioccipital.

Anterodorsally, there are prominent laterodorsally projecting clinoid processes connected to one another by a tall dorsum sellae (Figure 7b, c, f, cp, ds), similar to *Leptopleuron* (Spencer, 2000). The presence or absence of articulation with the prootic cannot be assessed, but the posterior margin of the clinoid processes are not as strongly convex as reconstructed for *Leptopleuron* (Spencer, 2000), and are beveled to face dorsolaterally. The clinoid processes have deeply incised grooves on their lateroventral surfaces, most likely to transport the internal carotid artery to the vidian canal. There is no indication of a second groove for the palatine branch of the facial nerve (VII), unlike the condition in *Leptopleuron* (Spencer, 2000). The foramina for the cerebral branches of the internal carotid arteries (Spencer, 2000) cannot be recognized, but the anterior part of the element has broken away. The pituitary fossa is divided in two by a very low midline ridge (Figure 7c). Behind the dorsum sellae, in the anterior part of the endocranial cavity, the basisphenoid is poorly ossified adjacent to its contact with the basioccipital.

The ventral surface of the basisphenoid is strongly concave, particularly towards the posterior end, forming the basisphenoid fossa (Figure 7e, bf). This fossa is funnel or V-shaped. There is no indication of a thin midline ridge as described for *Leptopleuron* (Spencer, 2000).

4.13 | Dentary

There are 10 dentaries, six from the left side (UMZC 2023.4.19, UMZC 2023.4.20, UMZC 2023.4.21, UMZC 2023.4.22, UMZC 2023.4.23, UMZC 2023.4.24) and four from the right side (UMZC 2023.4.25, UMZC 2023.4.26, UMZC 2023.4.27, UMZC 2023.4.28), although all are incomplete and missing at least the posteroventral portions of the bone (Figure 8). Where complete tooth count is known it is variable, with four in UMZC 2023.4.20 and UMZC 2023.4.22, but with five in UMZC 2023.4.21 and also inferred for UMZC 2023.4.19. In *Leptopleuron* (Säilä 2011) there are 5 or 6 dentary teeth, whereas *Hypsognathus* has 4 or 6 (Sues et al., 2000) and *Soturnia* has four (Cisneros & Schultz, 2003).

The first dentary tooth is only present in UMZC 2023.4.26 (Figure 8n) and has broken away in other specimens in which the anterior end of the dentary is preserved.

The tooth is monocuspid, incisiform, and procumbent, similar to that of *Hypsognathus* and *Leptopleuron* (Sues et al., 2000; Säilä 2011), although its size relative to the other dentary teeth is unclear. A short diastema is present between the first and second tooth in all specimens where this region is preserved (UMZC 2023.4.20, UMZC 2023.4.21, UMZC 2023.4.23, UMZC 2023.4.25, UMZC 2023.4.26, UMZC 2023.4.27, UMZC 2023.4.28), with the exception of UMZC 2023.4.22. This is one of the smaller specimens, and there does appear to be a tendency for the diastema to increase in length in larger specimens; as such, the absence of a diastema in UMZC 2023.4.22 may represent ontogenetic variation. A similar diastema is absent in *Hypsognathus*, *Soturnia* and *Leptopleuron* (Sues et al., 2000; Cisneros & Schultz, 2003; Säilä 2011) and appears to be an autapomorphy of *Hwiccewyrms*. Posterior to the diastema are 3 or 4 teeth (tooth positions 2–5), which are rounded and subtly bicuspid, although the distinction between the cusps is greatly reduced by wear, and not strongly labiolingually expanded (unlike the maxillary teeth). Posterodorsally facing wear surfaces are generally present on the crowns. The dentary crowns are distinct from those of *Leptopleuron* (Säilä 2011) in not being transversely expanded and being only subtly bicuspid, rather than clearly differentiated into lingual and labial cusps connected by a ridge. The dentary crowns of *Soturnia* are described as monocuspid and also appear to lack transverse expansion (Cisneros & Schultz, 2003), whereas details of the dentary teeth of *Hypsognathus* are not available (Sues et al., 2000). Details of tooth implantation are described below.

The dentary is shallowest dorsoventrally below the diastema and expands in dorsoventral height both anteriorly and posteriorly from this point, becoming particularly deep posteriorly (Figure 8a, d, k), similar to *Leptopleuron* (Säilä 2011) and *Hypsognathus* (Sues et al., 2000). There is a foramen on the lateral surface, positioned below the third tooth, at about the middle of the dorsoventral height of the bone (Figure 8a, d, for). The lateral surface is generally smooth and unsculptured. On the medial surface, the Meckelian groove is close to the ventral margin of the dentary and deepens in height posteriorly. Part of the coronoid process posterior to the tooth row is preserved in UMZC 2023.4.19, UMZC 2023.4.20, UMZC 2023.4.21 and UMZC 2023.4.22.

4.14 | Posterior hemimandible

A partial posterior left hemimandible is present (UMZC 2023.4.29; Figure 8o–q). This appears to represent the angular and some or all the articular. The angular is transversely compressed with the base of the internal adductor fossa preserved medially. Posteriorly, the articular region

is strongly transversely expanded but the glenoid is not well preserved.

4.15 | Tooth implantation and replacement

Premaxillary, maxillary, and dentary teeth are fused directly onto the tooth-bearing element through ankylosis (Figure 9c, h, i, m, q, u, x) with attachment (alveolar) bone that is distinct from tooth tissues and the rest of the bony element. The attachment bone appears highly vascularized with larger canals and a spongier structure than the lamellar bone of the tooth bearing elements (Figure 9h, i, m, q, u). There is growth of attachment bone anteriorly and posteriorly between the maxillary teeth, and to a lesser extent the dentary teeth. This gives the appearance that they are set in shallow sockets, especially when viewed in sagittal section (Figure 9m, u). However, this concavity is less the case in a coronal section through the maxillary and dentary teeth (Figure 9i), and the procumbent first dentary tooth (Figure 9x) and all premaxillary teeth (Figure 9c, h, m) appear shallowly set. Nevertheless, there are distinct dental alveoli left vacant where the fourth right maxillary tooth is missing in UMZC 2023.4.4 (Figure 4d, h) and a less distinct socket for the missing second right premaxillary tooth in UMZC 2023.4.1 (Figures 2c, 3c). The depth of these alveoli cannot fully be accounted for by dental tissues based on our CT-data for in-situ teeth (Figure 9c, h, i, m) and may be exaggerated by the large pulp cavities and by the removal of attachment bone that also would have surrounded the region. The presence of these alveoli and our CT-data lend support to a classification of tooth implantation as being deeper than a mode of acrodonty that is confined strictly to the margin of the jawbone, at least in the case of some of the dentition. We describe the tooth implantation in *Hwiccewyrn* as acrodont in a condition like that seen from histological work on other procolophonids (*Soturnia*; Cabreira & Cisneros, 2009)—the tooth base forming a short dentine pedicel anchored by attachment bone, though perhaps resembling protothecodonty in the posterior-most maxillary teeth. The use of these terms as they apply to procolophonids remains contentious (see Discussion).

The pulp cavity in all teeth is large and matches broadly the shape of the tooth crowns (Figure 9c, h, i, m, q, u, x), also being labiolingually expanded in the maxillary teeth (Figure 9i) and extends shortly beyond the extent of the dental tissues into the tooth bearing element (Figure 9m, u). The dentine layer is thick and the layer junction between the enamel and dentine of the tooth crowns can somewhat be delimited in the CT-images (Figure 9c, i, m, q, x).

Specimen UMZC 2023.4.2 shows ongoing tooth replacement of the second premaxillary tooth (Figure 9b–f). This tooth (which may be damaged anteriorly, Figure 9d, e) has thinned dentine where an extensive resorption pit is present at its lingual base, confluent with its pulp cavity, that has resorbed much of the attachment bone in this region (Figure 9b, c, m). In the resorption pit, a small developing replacement tooth, which is conical but open lingually and dorsally (Figure 9b, e, f, m), appears to be preparing to erupt labio-vertically as it is directed towards and into the pulp cavity of the tooth to be replaced (Figure 9c–f, m). A resorption pit also appears to be present towards the posterior of the medial side of the second dentary tooth in specimen UMZC.2023.4.21 (Figure 8e) but contains no visible replacement tooth when examined in CT images.

4.16 | Vertebrae

There are at least 15 elements that represent partial vertebrae within the collection of procolophonid specimens from Cromhall, of which nine represent isolated partial or complete centra, three neural arch fragments, a relatively complete neural arch, and two mostly complete vertebrae. There is a possible cervical centrum (UMZC 2023.4.30; Figure 10a–f). The two mostly complete vertebrae appear to represent dorsals (UMZC 2023.4.31, Figure 10m–r; UMZC 2023.4.32, Figure 10s–x), as does a nearly complete neural arch (UMZC 2023.4.33; Figure 10y–AD) and a well-preserved centrum (UMZC 2023.4.34; Figure 10g–l). Other specimens are highly incomplete and are not described or formally referred to *Hwiccewyrn* here.

The possible cervical centrum (UMZC 2023.4.30) is shorter anteroposteriorly than transversely wide in ventral view (Figure 10d). The anterior and posterior articular faces have oval outlines, being wider transversely than dorsoventrally high (Figure 10a, b), and are very deeply concave with a notochordal pit in the deepest part. On the ventral surface there are concave facets at anterior and posterior ends (Figure 10d, icfa), connected to one another by a short median ridge. The ventral borders of these facets are raised into distinct ridges. These facets are presumably for articulation with intercentra. Laterally there is a facet on the anterior end of the centrum for the cervical rib (Figure 10e, crfa), and the lateral surface of the centrum behind this facet is deeply concave and pierced in several places by foramina. Dorsally, the neural arch is missing, exposing the deep neural canal.

The dorsal vertebrae have centra that vary in proportions from approximately subequal in anteroposterior length and transverse width (UMZC 2023.4.32; Figure 10s–x) to anteroposteriorly longer than transversely wide (UMZC

2023.4.31, UMZC 2023.4.34; Figure 10g–r). The articular surfaces of the centra have subcircular to oval outlines and all the vertebrae are notochordal, with deeply concave articular surfaces pierced by the notochordal canal. The ventral margin of the centrum is smoothly rounded (Figure 10j, p, v), lacking a median ridge, differing from the condition in *Leptopleuron* (Säilä 2011), which possesses a median ridge flanked by grooves. Neurocentral sutures are clearly visible in *Hwiccewurm*. The lateral surfaces of the centra are pierced by at least two foramina, one placed anteriorly and one posteriorly, with the posterior foramen typically being the larger of the two.

The neural canals of the dorsal vertebrae have subcircular cross sections (Figure 10m, s). Prezygapophyses are large projections that extend anterior to the anterior margin of the centrum in lateral view. Their articular surfaces face dorsally and slightly medially. The facets for the dorsal ribs are dorsoventrally elongate and extend from immediately posterior to the posterior margin of the prezygapophyseal articular surface onto the anterodorsal corner of the centrum (e.g., Figure 10q, r). Posteriorly the postzygapophyses project beyond the posterior margin of the centrum in lateral view and have articular surfaces that face almost entirely ventrally, and slightly laterally. The neural spine is not complete in any specimen, but appears to have been a tapering, posterodorsally inclined projection (e.g., Figure 10q, r, AC, AD). The anterior margin of the spine is drawn out into a sharp ridge. A sharp ridge also descends ventrally from the posterior margin of the spine, in between the postzygapophyses.

4.17 | Ribs

There are four partial ribs preserved, two from the left side (UMZC 2023.4.35, UMZC 2023.4.36; Figure 11a–d) and two from the right side (UMZC 2023.4.37, UMZC 2023.4.38; Figure 11e–h). All of them are missing their distal ends but their proximal ends are generally well preserved. All appear to be dorsal ribs. In all cases the head is holocephalous and not clearly subdivided into a capitulum and tuberculum. The heads are all dorsoventrally expanded relative to the shafts (as for *Leptopleuron*; Säilä 2011), although there is some variation with UMZC 2023.4.38 having a head that is particularly strongly dorsally expanded (Figure 11g, h). In proximal view, there are two transversely expanded articular surfaces, one placed dorsally and one ventrally, separated by a transversely compressed sheet of bone. The dorsoventral depth of the rib shaft is uniform for the first third to half of its preserved length, and then the shaft tapers gently distally. The shafts are anteroposteriorly compressed with a shallow median groove on the posterior surface that is confluent with a sulcus on the posterior surface of the head

between the two proximal articular surfaces. There is a ridge on the anterior surface of the shaft in all four ribs (Figure 11a, c, e, g) although there is variation in the morphology of this. In UMZC 2023.4.36 and UMZC 2023.4.37 the ridge is anterodorsally positioned (Figure 11c, e), whereas in UMZC 2023.4.35 it is placed in a more median position on the anterior surface and has a small facet close to the proximal end of the shaft that may be linked to the position of the pectoral girdle (Figure 11a). The rib shafts are curved along their length but there appears to be some variation in the degree of curvature. In UMZC 2023.4.35 there is a very distinct inflection of the head relative to the shaft at the proximal end (Figure 11a, b).

Either all dorsal ribs in this taxon are holocephalous (as in *Procolophon trigoniceps*, deBraga, 2003; *Sauropareion*, MacDougall et al., 2013) or the ribs represent more posterior dorsal ribs in a condition where only the anteriormost dorsal ribs are dichcephalous (*Soturnia*, Cisneros & Schultz, 2003; *Kapes bentoni*, Zaher et al., 2019).

4.18 | Interclavicle

A single partial interclavicle is preserved (UMZC 2023.4.39; Figure 12a, b). This is an anchor-like or T-shaped element, most of the right side of which is preserved, but lacking most of the left side. The median process is incomplete at its posterior end and lacks its left margin. However, the median ridge on the ventral surface of the median process and the right margin of the process are parallel to one another suggesting that the median process had a consistent width along its preserved length. The ventral surface of the median process is slightly ventrally convex both along its length and transversely and has a central raised ridge on the anterior half of its length which fades out posteriorly (Figure 12a, mri). This differs from the situation in *Procolophon* (deBraga, 2003) and *Kapes bentoni* (Zaher et al., 2019) in which the ridge continues until close to the distal end of the bone. The median ridge of *Hwiccewurm* increases in prominence anteriorly and sharply merges into the raised ridge demarcating the anteroventral margins of the lateral processes. The lateral margins of the median process curve smoothly to meet the posterior margins of the lateral processes. There is a distinct anterodorsally facing concave facet for articulation with the clavicle on the lateral process (Figure 12b, fa). Towards its end the lateral process curves slightly posterodorsally.

4.19 | Scapula

A partial right scapula (UMZC 2023.4.40; Figure 12c–e) is preserved, but is missing the distal part of the blade and is damaged proximally where it would have articulated

with the coracoid. The scapula blade is rectangular in lateral view (Figure 12c) and curved along its length, with posterior and anterior margins forming sharp ridges. The scapular contribution to the glenoid is subcircular and concave (Figure 12c, gl). The lateral surface of the proximal end is depressed above the glenoid. A supraglenoid foramen cannot be identified although there is a shallow depression adjacent to the posterolateral edge of the supraglenoid buttress. There is a low convexity on the medial surface of the element that runs from the medial margin of the glenoid up along the midline of the scapula blade. This convexity is separated from the ridge that forms the posterior margin of the blade by a groove.

4.20 | Metacoracoid

A mostly complete left metacoracoid (UMZC 2023.4.41; Figure 12f–h) is preserved but is moderately damaged along the region where it would have articulated with the procoracoid. The main part of the metacoracoid is transversely compressed and fan-like, but is transversely expanded adjacent to its contact with the scapula to form a substantial glenoid facet (Figure 12h, cgl), which has a strongly concave surface.

4.21 | Humerus

Three left humeri are preserved with a substantial range in size. The largest humerus (UMZC 2023.4.42; Figure 13a–f) and the middle sized one (UMZC 2023.4.43; Figure 13g–l) are mostly complete (the deltopectoral crest is damaged in UMZC 2023.4.42), whereas the smallest specimen (UMZC 2023.4.44) is missing most of the proximal end. The humerus appears more gracile than that of *Procolophon* (deBraga, 2003), with a less marked expansion from the narrow midshaft into the proximal and distal ends. It is approximately twice as long as the maximum widths of the proximal and distal ends. The maximum expansions of the proximal and distal ends are twisted relative to each other at an angle of approximately 45–50°, similar to the condition in *Procolophon* (deBraga, 2003) and *Leptopleuron* (Säilä 2011). The maximum expansion of the distal end is only slightly greater than that of the proximal end. The deltopectoral crest is relatively weakly developed, transversely narrow, proximally positioned and continuous with the articular surface of the head (Figure 13b, d, h, j), as opposed to the much more robust, thickened and distally offset deltopectoral crest in *Procolophon* (deBraga, 2003) and *Kapes* (Zaher et al., 2019). The position and size of the deltopectoral crest make the proximal humeral head almost symmetrical in posterior view in

H. trispiculum. A deep sulcus on the posterior surface of the proximal end separates the deltopectoral crest from the facet for articulation with the glenoid. Distally there is a large entepicondylar foramen (Figure 13a–d, g, i) but the ectepicondylar foramen is absent, as in other procolophonids (Cisneros, 2008). The entepicondyle extends only marginally more distally than the ectepicondyle and is more rounded than in *Procolophon* (deBraga, 2003) and lacks a pronounced entepicondylar process (sensu Cisneros, 2008). The distal end is therefore more symmetrical in posteroventral view than *Procolophon* (deBraga, 2003) and more like that of *Leptopleuron* (Säilä, 2010). The capitulum and trochlear are weakly developed and poorly defined. The distal end is strongly recessed and concave above the condyles in posteroventral view (Figure 13a). There is a much shallower depression present between the condyles in anterodorsal view (Figure 13c).

4.22 | Radius

A single left radius is preserved (UMZC 2023.4.45; Figure 13m–r), missing part of the proximal end. It is relatively slender with a straight shaft, with gentle expansions of the proximal and distal end relative to the shaft. The bone including the shaft is transversely compressed with a gently convex lateral surface and a flattened medial surface.

4.23 | Ilium

Three ilia are preserved, two left (one large and one very small, UMZC 2023.4.46 and UMZC 2023.4.47; Figure 14a–d) and one right (UMZC 2023.4.48; slightly smaller than the large left ilium; Figure 14e, f), representing three individuals. The ilium is anteroposteriorly constricted at a point level with the dorsal rim of the acetabulum then flares dorsally into an dorsoventrally tall, fan shaped blade (Figure 14a–d), the anterodorsal corner of which is not preserved in any specimen. The ilium is much taller than in *Procolophon* (deBraga, 2003). Although poorly preserved, the iliac blade of *Leptopleuron* is also dorsoventrally tall (Säilä, 2010). The dorsal edge of the iliac blade is poorly preserved but gently convex in lateral view. UMZC 2023.4.46 in particular displays extensive pitting over much of the surface of the blade: this pitting is more linear towards the dorsal extent of the lateral surface and at the dorsal and ventral extremities of the medial surface. There is a broad depressed area for sacral rib attachment on the medial surface of the blade (Figure 14b, d, srf). This area is deepest anteriorly and tapers posterodorsally and is demarcated posteroventrally by a low ridge. The dorsal margin of the acetabulum has a well-defined rim. The

acetabulum opens ventrally, confluent with a rounded triangular ventral projection of bone. There is a low buttress on the lateral surface, confluent with the anterior rim of the acetabulum, and a raised irregular surface anterodorsal to the acetabulum, the latter representing a site of muscle attachment. Anterior and posterior to the acetabulum, the ventral part of the ilium forms two sharp triangular projections, the anterior one is larger and as a result the portion of the iliac blade anterior to the acetabulum is broader than that posterior to the acetabulum. Dorsal to these anterior and posterior projections of the ilium base the iliac blade has a very slightly convex anterior margin and a distinctly concave posterior edge.

4.24 | Ischium

A partial left ischium is preserved (UMZC 2023.4.49; Figure 14g–i), which articulates reasonably well with the large left ilium (UMZC 2023.4.46), suggesting that they may represent a single individual. The element is generally strongly transversely compressed forming a plate-like blade but is thickened into a head dorsolaterally where it contacted the ilium. Just under half of the proximal surface of the head forms an articular surface for the ilium (Figure 14h, i, ilfa), whereas the other half forms the contribution of the ischium to the acetabulum (Figure 14g, i, isac). Although the ventromedial margin of the blade is incomplete, the ventral surface of the ischium is gently concave transversely and lacks any indication of the ventral depressions that were considered an autapomorphy of *Leptopleuron* (Säilä, 2010). There is a distinct thickening on the dorsal surface of the blade forming a low ridge set towards its anterior margin and close to the midline (Figure 14h).

4.25 | Femur

One left femur (larger; UMZC 2023.4.50; Figure 15a–f) and one right femur (smaller; UMZC 2023.4.51; Figure 15g–i) are preserved. There is damage to the proximal head of UMZC 2023.4.51, and damage to the distal ends of both elements. The femur is a relatively elongate and slender bone, more slender than in *Procolophon* (deBraga, 2003) but similar to that of *Leptopleuron* (Säilä, 2010). The femur has a sigmoidal curvature in anterior and posterior views, similar to *Procolophon* and *Leptopleuron*, such that the proximal head is deflected dorsally although not as strongly as in *Procolophon* (deBraga, 2003). The internal trochanter is large and closely linked with the proximal head of the femur (differing from the condition in

Procolophon in which the internal trochanter is offset distally: deBraga, 2003), projecting smoothly from it distoventrally (Figure 15b, d, h, j). The adductor ridge linked with the internal trochanter is expanded and has a distinctly convex edge in anterior view (unlike in *Procolophon* where it is straighter, deBraga, 2003) and terminates around the mid-shaft point (Figure 15b, d, h). It has a pitted surface texture similar to the condition in *Procolophon* (deBraga, 2003), with this pitting most strongly developed posteriorly and ventrally, presumably the insertion site for much of the *M. caudofemoralis*. The distal ends of both specimens are poorly preserved. The popliteal fossa is poorly preserved but the tibial facets are clearly separated by a wedge shaped intercondylar fossa that has a pitted surface texture (Figure 15c, i).

4.26 | Phylogenetic results

Analysis 1 using equal weights recovered 706 most parsimonious trees (MPTs) of 160 steps. The strict consensus of these trees shows a very large polytomy at the base of Procolophonidae (Figure 16a). There is a clade resolved that comprises Leptopleuroninae + Procolophoninae + *Eumetabolodon bathycephalus*. *Hwiccewurm* falls out in a derived position within Leptopleuroninae in a polytomy with *Hypsognathus*, *Soturnia* and *Leptopleuron*. The strict consensus tree resembles that of Hamley et al. (2021:Figure 2a) but differs in the less resolved position of *Coletta*, a change in the position of *Neoprocolophon*, which in our tree is recovered in a polytomy at the base of Leptopleuroninae, and a lack of resolution between *Hypsognathus*, *Soturnia* and *Leptopleuron*. Bootstrap frequencies show moderate support (53%) for a *Hypsognathus* + *Soturnia* clade to the exclusion of *Hwiccewurm* and *Leptopleuron*. The clade including *Hwiccewurm*, *Hypsognathus*, *Soturnia* and *Leptopleuron* is supported by three unambiguous synapomorphies: reduction to five or fewer maxillary teeth (Character 32, state 4); maxillary teeth with a deep occlusal basin (Character 39, state 1); molariform dentary teeth with two very close tooth cusps (Character 41, state 1).

Analysis 2 recovered a single MPT (best score: 14.06). The tree (Figure 16b) shows similarities in major patterns to that found by analysis 2 of Hamley et al. (2021:Figure 2b), but with differences in the positions of individual taxa. Leptopleuroninae is much more taxonomically inclusive in this analysis. *Hwiccewurm* is placed outside of a clade comprising *Leptopleuron* + (*Hypsognathus* + *Soturnia*).

Analysis 3 recovered 18 MPTs of 157 steps. The strict consensus tree (Figure 16c) is identical to that of

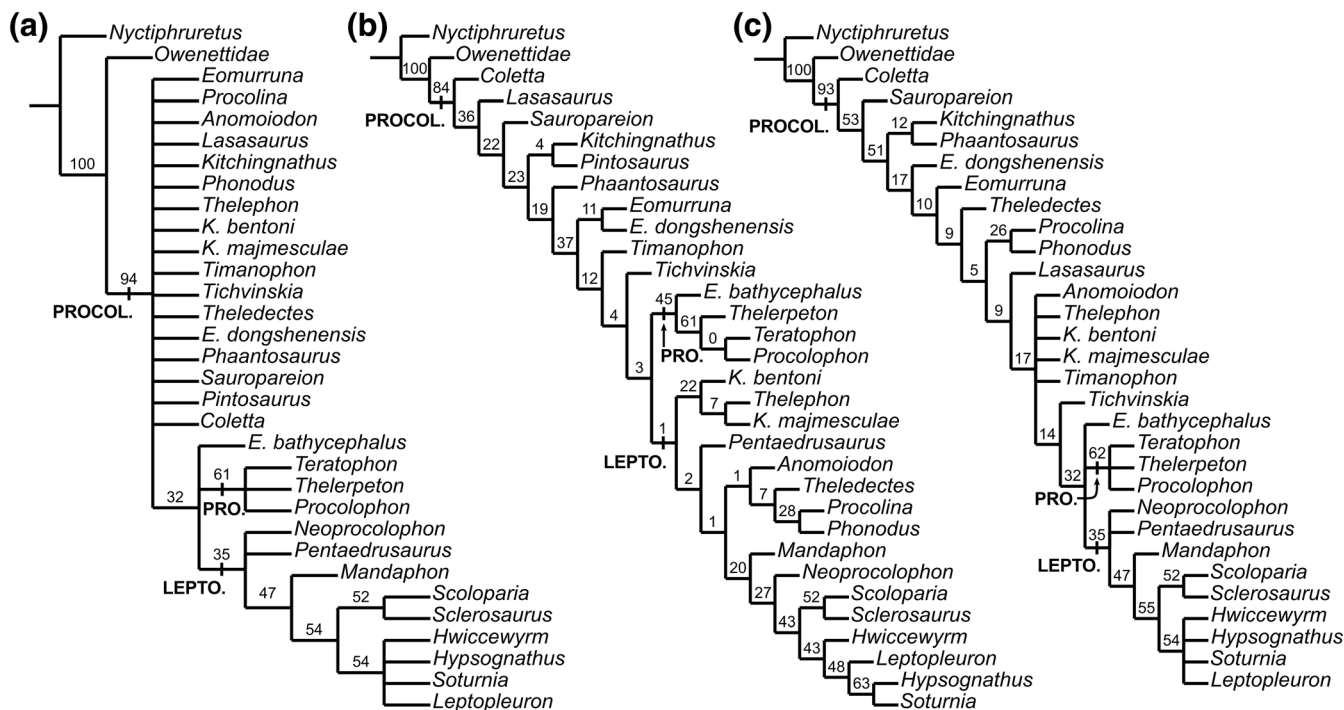


FIGURE 16 Results of the phylogenetic analyses testing the phylogenetic position of *Hwiccewurm trispiculum* gen et sp. nov. (a) Strict consensus of 760 most parsimonious trees (MPTs) recovered by analysis 1. (b) Single MPT produced by analysis 2. (c) Strict consensus of 18 MPTs produced by analysis 3. Numbers above branches show bootstrap support. LEPTO., Leptopleuroninae; PRO., Procolophoninae; PROCOL., Procolophonidae.

Hamley et al. (2021:Figure 2c), with the exception of a sister-taxon relationship between *Scoloparia* and *Sclerosaurus*. *Hwiccewurm* is recovered in a derived position within Leptopleuroninae in a polytomy with *Hypsognathus*, *Soturnia* and *Leptopleuron*. The characters providing unambiguous support for this clade are the same as in Analysis 1.

5 | DISCUSSION

5.1 | Procolophonids in the fissure fills

The only other procolophonid material to be formally described from the Late Triassic fissure fills is from the Ruthin fissure of South Wales (Edwards, 2000; Edwards & Evans, 2006; Skinner et al., 2020). Edwards and Evans (2006) provided a brief overview of the assemblage (based upon the unpublished PhD of Edwards, 2000) and considered it to be dominated by an unnamed armored leptopleuronine similar to *Scoloparia* (Sues & Baird, 1998) with rare remains of *Haligonia* sp. Skinner et al. (2020) described four genera as present at Ruthin, comprising *Haligonia* cf. *bolodon*, cf. *Scoloparia* sp., *Smilodonterpeton ruthinensis*, and a leptopleuronine considered similar to both *Hypsognathus* and *Leptopleuron*.

Haligonia is clearly distinct from *Hwiccewurm* in the position of four small anterior teeth in the maxilla followed by a greatly enlarged fifth tooth with a massive bulbous crown (Skinner et al., 2020; Sues & Baird, 1998). Material referred to cf. *Scoloparia* sp. from Ruthin by Skinner et al. (2020) consists of poorly preserved premaxillae and two isolated, elongate cephalic spines, as well as numerous osteoderms that might represent the same taxon. The referral of the material to *Scoloparia* by Skinner et al. (2020) was based primarily upon the presence of three premaxillary teeth, given that only two are present in most Late Triassic procolophonids, but the character is polymorphic in *Scoloparia*, with some specimens having two premaxillary teeth and others three (Sues & Baird, 1998). The association of the Ruthin cephalic spines with the premaxillae is unclear, and no clear rationale was provided for the identification of the osteoderms as procolophonid. The Ruthin material does not preserve autapomorphic features of *Scoloparia*, and the distinctive chisel-like posterior crowns of the maxilla and dentary of *Scoloparia* (Sues & Baird, 1998) are as yet unknown at Ruthin. As such, we consider the presence of *Scoloparia* at Ruthin to be questionable, but, in any case, *Hwiccewurm* can be clearly distinguished from the material referred to cf. *Scoloparia* sp. at Ruthin based on possession of only two premaxillary teeth in the former.

Skinner et al. (2020) described *Smilodonterpeton ruthinensis* as a new procolophonid taxon from the Ruthin fissure on the basis of 13 dentary fragments and one incomplete maxilla, characterized by the presence of posterior dentary teeth that appear square in labial or lingual view, deep grooves on the mesial and distal bases of the dentary teeth, and a dorsoventrally shallow dentary with a deep Meckelian canal. *Hwiccewyrms* clearly differs from *Smilodonterpeton* in possessing posterior dentary teeth that are conical in labial and lingual views, sub-circular in occlusal view, and which lack deep mesial and distal grooves, and in possessing a dentary that becomes very deep dorsoventrally posteriorly.

The final taxon described by Skinner et al. (2020) was an unnamed species represented by isolated premaxillae, dentaries and maxillary teeth that they considered similar to the leptopleuronines *Hypsognathus* and *Leptopleuron*. These remains from Ruthin show similarities to those of *Hwiccewyrms* and other leptopleuronines, although the premaxillary teeth appear more conical and less bulbous in labial view in the Ruthin form, lingual and labial cusps of maxillary teeth are generally similarly developed in *Hwiccewyrms* rather than the labial cusp being enlarged as in the Ruthin material, and a diastema between the first and second dentary teeth is absent in the Ruthin material. Thus, it seems likely that the Ruthin material is at least specifically distinct from *Hwiccewyrms*.

Hwiccewyrms is the most completely known procolophonid taxon known to date from the fissure fills of south-west England and South Wales. The Ruthin fissure appears to preserve at least three distinct procolophonid species, but all of these can be clearly differentiated from *Hwiccewyrms*. Although Skinner et al. (2020) considered the Ruthin fissure to be of most likely early Rhaetian age, *Haligonia*, *Scoloparia* and *Leptopleuron* are all known from strata of Carnian age elsewhere (Säilä, 2010; Sues & Baird, 1998), and Edwards and Evans (2006) considered the assemblage to likely date to the late Carnian. In our phylogenetic analysis *Hwiccewyrms* is placed within a clade of derived leptopleuronines known from late Carnian (*Leptopleuron*) through to late Norian–Rhaetian (*Hypsognathus*) and so is of limited use in constraining the disputed ages of the infillings of the Cromhall fissures.

5.2 | Body size evolution

Skinner et al. (2020) suggested that many of the taxa found at Ruthin and other Late Triassic fissures such as Cromhall were unusually small compared to close relatives found in other Late Triassic sites globally, and that given a hypothesis that these fissures formed in island settings, this might represent the oldest evidence in the

fossil record of insular island dwarfism. However, this hypothesis lacked an explicit phylogenetic context and has been subsequently challenged on the basis that key taxa from the fissure fills may simply be plesiomorphically small (Foffa et al., 2023; Spiekman et al., 2021; Sues & Schoch, 2023). Indeed, even the proposed island setting may be considered suspect if the fissure sites are older than Rhaetian in age (and thus predate the Rhaetian transgression). The holotype of *H. trispiculum* has a maxilla with an anteroposterior length of ~15 mm, which based on comparison to *Leptopleuron* (Säilä, 2010) would suggest a total basal skull length of ~60 mm. This is comparable to closely related species such as *Leptopleuron* (skull length 55 mm; Säilä, 2010) and *Hypsognathus* (skull length 50–75 mm; Sues et al., 2000). Although detailed analysis of body size evolution in procolophonids in a phylogenetic context has yet to be conducted, *Hwiccewyrms* is clearly not unusually small relative to other members of the clade, and the wider hypothesis of island dwarfism in the fissure fill assemblages appears to have limited support to date.

5.3 | Tooth replacement

The nature of tooth implantation in procolophonids has been contentious with taxa classified as protothecodont (Gow, 1977; MacDougall & Modesto, 2011; Säilä, 2009; Small, 1997; Sues et al., 2000), acrodont (Cabreira & Cisneros, 2009; Hamley et al., 2021; Skinner et al., 2020) or combining both modes (Jenkins & Bhullar, 2022). The matter is complicated by ambiguous and inconsistent definition of terms (Bertin et al., 2018; Haridy, 2018; Jenkins & Bhullar, 2022) and comparison with characteristics of tooth implantation in extant groups that may be highly derived features (lepidosaurian acrodonty; Haridy et al., 2018).

In contrast to protothecodonty or ankylothecodonty, defined as teeth with roots fused into sockets (Bertin et al., 2018; Cabreira & Cisneros, 2009; Small, 1997; Sues & Olsen, 1993), a definition of acrodonty as teeth ankylosed to the “apex” of the jaw better fits the dentition of *Hwiccewyrms* which lacks clearly rooted implantation. However, the condition is not unambiguous considering vacant dental alveoli (Figures 2c, 4h) and the somewhat root-like appearance of the larger maxillary and dentary teeth in sagittal section (Figure 9m, u), resulting from attachment bone deposited anteriorly and posteriorly between the teeth. This may function to secure the teeth not only to the bony element but also to each other and a similar condition exists in other taxa with dentition described as acrodont (Haridy, 2018). Our CT data closely resemble the dental implantation described from

histological work by Cabreira and Cisneros (2009) on *Soturnia*, where the teeth exhibit a “low pedicle” which cannot confidently be characterized as a root, also described as acrodont. Combinations of superficially acrodont features (high lingual walls of the dentary, fusion to the summit of the tooth bearing element) with protothecodont features (sockets or dental alveoli, extensive pulp cavities) has led to the suggestion of a mode of “pseudo-acrodont” implantation in procolophonids (Falconnet et al., 2012; MacDougall & Modesto, 2011) in which modified protothecodonty mimics acrodonty in gross morphology.

The presence of tooth replacement in the procolophonid *Sauropareion* was another factor that led MacDougall and Modesto (2011) to tentatively classify its tooth implantation as protothecodont (on the basis that modern acrodont taxa lack tooth replacement). However, tooth replacement has been described in the oldest known tetrapod with an acrodont dentition (the Early Permian captorhinid *Opisthodontosaurus*) and a lack of replacement in some modern acrodont groups is a secondarily derived feature (Haridy et al., 2018). Tooth replacement therefore does not preclude a classification of *Hwiccewyrms* as acrodont. Instances of tooth replacement involving resorption pits in procolophonids are well documented but infrequent (Hamley et al., 2021; MacDougall & Modesto, 2011; Säilä, 2009; Small, 1997). Typically, only a single maxillary (Hamley et al., 2021) or dentary (MacDougall & Modesto, 2011; Small, 1997) tooth is preserved as being replaced in the element at any one time. Among 17 tooth bearing specimens of *Hwiccewyrms*, only the premaxilla of UMZC 2023.4.2 shows ongoing tooth replacement (along with the possible resorption pit of UMZC 2023.4.21) and this may be the first described instance of the ongoing replacement of a premaxillary tooth among procolophonids. The rarity of tooth replacement in *Hwiccewyrms* and other described procolophonid remains may suggest a low rate of tooth replacement (Gow, 1977; Li, 1983), potentially linked with a trend towards more massive, resistant teeth that are reduced in number (Cabreira & Cisneros, 2009).

AUTHOR CONTRIBUTIONS



Richard J. Butler: Conceptualization; formal analysis; investigation; methodology; project administration; supervision; visualization; writing – original draft; writing – review and editing. **Luke E. Meade:** Data curation; formal analysis; investigation; visualization; writing – original draft; writing – review and editing. **Terri J. Cleary:** Investigation; writing – review and editing. **Kai T. McWhirter:** Investigation; writing – review and editing. **Emily E. Brown:** Investigation; visualization; writing – review and editing. **Tom S. Kemp:**

Writing – review and editing. **Juan Benito:** Writing – review and editing. **Nicholas C. Fraser:** Investigation; writing – review and editing.

ACKNOWLEDGMENTS

We thank Mathew Lowe and Jason Head (UMZC), Alex Brasier (AUP), and Marc Jones and Mike Day (Natural History Museum, London) for access to specimens. Thanks to Susan Evans for facilitating this project. Mike Simms provided useful discussion of the age of the fissure fill localities. Tom Davies is thanked for conducting CT scanning at the University of Bristol. We thank the Willi Hennig Society for providing free access to TNT software. Hans-Dieter Sues, an anonymous reviewer and the editor Felipe Pinheiro provided helpful comments that improved the final manuscript.

ORCID

Richard J. Butler  <https://orcid.org/0000-0003-2136-7541>
 Luke E. Meade  <https://orcid.org/0000-0001-7829-5193>
 Terri J. Cleary  <https://orcid.org/0000-0003-0424-8073>
 Emily E. Brown  <https://orcid.org/0000-0003-3491-5586>
 Juan Benito  <https://orcid.org/0000-0003-4497-2058>
 Nicholas C. Fraser  <https://orcid.org/0000-0003-4408-4640>

REFERENCES

- Bertin, T. J. C., Thivichon-Prince, B., LeBlanc, A. R. H., Caldwell, M. W., & Viriot, L. (2018). Current perspectives on tooth implantation, attachment, and replacement in Amniota. *Frontiers in Physiology*, 9, 1630.
- Cabreira, S. F., & Cisneros, J. C. (2009). Tooth histology of the parareptile *Soturnia caliodon* from the Upper Triassic of Rio Grande do Sul, Brazil. *Acta Palaeontologica Polonica*, 54, 743–748.
- Carroll, R. L., & Lindsay, W. (1985). Cranial anatomy of the primitive reptile *Procolophon*. *Canadian Journal of Earth Sciences*, 22, 1571–1587.
- Cisneros, J. C. (2008). Phylogenetic relationships of procolophonid parareptiles with remarks on their geological record. *Journal of Systematic Palaeontology*, 6, 345–366.
- Cisneros, J. C., & Ruta, M. (2010). Morphological diversity and biogeography of procolophonids (Amniota: Parareptilia). *Journal of Systematic Palaeontology*, 8, 607–625.
- Cisneros, J. C., & Schultz, C. L. (2003). *Soturnia caliodon* n. g. n. sp., a procolophonid reptile from the Upper Triassic of southern Brazil. *Neues Jahrbuch für Geologie Und Paläontologie, Abhandlungen*, 227, 365–380.
- De Braga, M. (2003). The postcranial skeleton, phylogenetic position, and probable life style of the Early Triassic reptile *Procolophon trigoniceps*. *Canadian Journal of Earth Sciences*, 40, 527–556.
- Edwards, B. (2000). The Upper Triassic microvertebrate assemblage of Ruthin Quarry, South Wales. PhD, University College London, 390 pp.
- Edwards, B., & Evans, S. E. (2006). A Late Triassic microvertebrate assemblage from Ruthin Quarry, Wales. In P. M. Barrett & S. E.

- Evans (Eds.), *Ninth international symposium on Mesozoic terrestrial ecosystems and biota, abstracts and proceedings* (pp. 33–35). Natural History Museum.
- Falconnet, J., Andriamihaja, M., Läng, É., & Steyer, J.-S. (2012). First procolophonid (Reptilia, Parareptilia) from the Lower Triassic of Madagascar. *Comptes Rendus Palevol*, 11, 357–369.
- Foffa, D., Nesbitt, S. J., Kligman, B. T., Butler, R. J., & Stocker, M. R. (2023). New specimen and redescription of *Anisodontosaurus greeri* (Moenkopi Formation: Middle Triassic) and the spatiotemporal origins of Trilophosauridae. *Journal of Vertebrate Paleontology*, 43, e2220015.
- Fraser, N. C. (1982). A new rhynchocephalian from the British Upper Trias. *Palaeontology*, 25, 709–725.
- Fraser, N. C. (1985). Vertebrate faunas from Mesozoic fissure deposits of south west Britain. *Modern Geology*, 9, 273–300.
- Fraser, N. C. (1986a). Terrestrial vertebrates at the Triassic-Jurassic boundary in south west Britain. *Modern Geology*, 10, 147–157.
- Fraser, N. C. (1986b). New Triassic sphenodontids from south-west England and a review of their classification. *Palaeontology*, 29, 165–186.
- Fraser, N. C. (1988a). The osteology and relationships of *Clevo-saurus* (Reptilia: Sphenodontida). *Philosophical Transactions of the Royal Society of London*, B321, 125–178.
- Fraser, N. C. (1988b). Rare tetrapod remains from the Late Triassic fissure infillings of Cromhall Quarry, Avon. *Palaeontology*, 31, 567–576.
- Fraser, N. C. (1988c). Latest Triassic terrestrial vertebrates and their biostratigraphy. *Modern Geology*, 13, 125–140.
- Fraser, N. C. (1994). Assemblages of small tetrapods from British Late Triassic fissure deposits. In N. C. Fraser & H.-D. Sues (Eds.), *In the shadow of the dinosaurs* (pp. 214–226). Cambridge University Press.
- Fraser, N. C., Irmis, R. B., & Elliott, D. K. (2005). A procolophonid (Parareptilia) from the Owl Rock Member, Chinle Formation of Utah, USA. *Palaeontologia Electronica*, 8, 1–7.
- Fraser, N. C., Padian, K., Walkden, G. M., & Davis, A. L. M. (2002). Basal dinosauriform remains from Britain and the diagnosis of the Dinosauria. *Palaeontology*, 45, 79–95.
- Fraser, N. C., & Renesto, S. (2005). Additional drepanosaur elements from the Triassic fissure infills of Cromhall Quarry, England. *Jeffersoniana*, 15, 1–16.
- Fraser, N. C., & Walkden, G. M. (1983). The ecology of a Late Triassic reptile assemblage from Gloucestershire, England. *Palaeogeography, Palaeoclimatology, Palaeoecology*, 42, 341–365.
- Fraser, N. C., & Walkden, G. M. (1984). The postcranial skeleton of the Upper Triassic sphenodontid *Planocephalosaurus robinsonae*. *Palaeontology*, 27, 575–595.
- Goloboff, P. A., Carpenter, J. M., Arias, J. S., & Esquivel, D. R. (2008). Weighting against homoplasy improves phylogenetic analysis of morphological data sets. *Cladistics*, 24, 758–773.
- Goloboff, P. A., & Morales, M. M. (2023). TNT version 1.6, with a graphical interface for MacOS and Linux, including new routines in parallel. *Cladistics*, 39, 144–153.
- Gow, C. E. (1977). Tooth function and succession in the Triassic reptile *Procolophon trigoniceps*. *Palaeontology*, 20, 695–704.
- Halstead, L. B., & Nicoll, P. G. (1971). Fossilized caves of Mendip. *Studies in Speleology*, 2, 93–102.
- Hamley, T., Cisneros, J. C., & Damiani, R. (2021). A procolophonid reptile from the Lower Triassic of Australia. *Zoological Journal of the Linnean Society*, 192, 554–609.
- Haridy, Y. (2018). Histological analysis of post-eruption tooth wear adaptations, and ontogenetic changes in tooth implantation in the acrodontan squamate *Pogona vitticeps*. *PeerJ*, 6, e5923.
- Haridy, Y., LeBlanc, A. R., & Reisz, R. R. (2018). The Permian reptile *Opisthodontosaurus carrolli*: A model for acrodont tooth replacement and dental ontogeny. *Journal of Anatomy*, 232, 371–382.
- Ivakhnenko, M. F. (1979). Permian and Triassic procolophonians of the Russian platform. *Trudy Paleontologicheskogo Instituta, Akademiia Nauka SSSR*, 164, 1–80.
- Jenkins, K. M., & Bhullar, B. A. S. (2022). Tooth implantation and attachment in *Scoloparia glyphanodon* (Parareptilia: Procolophonidae). *Bulletin of the Peabody Museum of Natural History*, 63, 27–30.
- Laurin, M., & Reisz, R. R. (1995). A reevaluation of early amniote phylogeny. *Zoological Journal of the Linnean Society*, 113, 165–223.
- Li, J. (1983). Tooth replacement in a new genus of procolophonid from the Early Triassic of China. *Palaeontology*, 26, 567–583.
- Li, J. (1989). A new genus of Procolophonidae from the Lower Triassic of Shaanxi, China. *Vertebrata Palasiatica*, 27, 248–267.
- Lucas, S. G., Heckert, A. B., Fraser, N. C., & Huber, P. (1999). *Aetosaurs* from the upper Triassic of Great Britain and its biochronological significance. *Neues Jahrbuch für Geologie Und Paläontologie, Monatshefte*, 1999, 568–576.
- MacDougall, M. J., Brocklehurst, N., & Fröbisch, J. (2019). Species richness and disparity of parareptiles across the end-Permian mass extinction. *Proceedings of the Royal Society B*, 286, 20182572.
- MacDougall, M. J., & Modesto, S. P. (2011). New information on the skull of the Early Triassic parareptile *Sauropareion anoplus*, with a discussion of tooth attachment and replacement in procolophonids. *Journal of Vertebrate Paleontology*, 31, 270–278.
- MacDougall, M. J., Modesto, S. P., & Botha-Brink, J. (2013). The postcranial skeleton of the Early Triassic parareptile *Sauropareion anoplus*, with a discussion of possible life history. *Acta Palaeontologica Polonica*, 58, 737–749.
- Modesto, S. & Damiani, R. J. 2003. Taxonomic status of *Thelegnathus browni* Broom, a procolophonid reptile from the South African Triassic. *Annals of the Carnegie Museum* 72: 53–64.
- Modesto, S., Scott, D. M., Botha-Brink, J., & Reisz, R. R. (2010). A new and unusual procolophonid parareptile from the Lower Triassic Katberg Formation of South Africa. *Journal of Vertebrate Paleontology*, 30, 715–723.
- Modesto, S., Sues, H.-D., & Damiani, R. (2001). A new Triassic procolophonoid reptile and its implications for procolophonoid survivorship during the Permo-Triassic extinction event. *Proceedings of the Royal Society B*, 268, 2047–2052.
- Morton, J. D., Whiteside, D. I., Hethke, M., & Benton, M. J. (2017). Biostratigraphy and geometric morphometrics of conchostracans (Crustacea, Branchiopoda) from the Late Triassic fissure deposits of Cromhall Quarry, UK. *Palaeontology*, 60, 349–374.
- Mussini, G., Whiteside, D. I., Hildebrandt, C., & Benton, M. J. (2020). Anatomy of a Late Triassic Bristol fissure: Tytherington fissure 2. *Proceedings of the Geologists' Association*, 131, 73–93.

- O'Brien, A., Whiteside, D. I., & Marshall, J. E. A. (2018). Anatomical study of two previously undescribed specimens of *Clevosaurus hudsoni* (Lepidosauria: Rhynchocephalia) from Cromhall Quarry, UK, aided by computed tomography, yields additional information on the skeleton and hitherto undescribed bones. *Zoological Journal of the Linnean Society*, 183, 163–195.
- Olson, E. C. (1947). The family Diadectidae and its bearing on the classification of reptiles. *Fieldiana, Geology*, 11, 1–53.
- Piñeiro, G., Rojas, A., & Ubilla, M. (2004). A new procolophonoid (Reptilia, Parareptilia) from the Upper Permian of Uruguay. *Journal of Vertebrate Paleontology*, 24, 814–821.
- Pinheiro, F. L., Silva-Neves, E., & Da-Rosa, Á. A. S. (2021). An early-diverging procolophonid from the lowermost Triassic of South America and the origins of herbivory in Procolophonoida. *Papers in Palaeontology*, 7, 1601–1612.
- Renesto, S., & Fraser, N. C. (2003). Drepanosaurid (Reptilia: Diapsida) remains from a Late Triassic infilling at Cromhall Quarry (Avon, Great Britain). *Journal of Vertebrate Paleontology*, 23, 703–705.
- Robinson, P. L. (1957). The Mesozoic fissures of the Bristol Channel area and their vertebrate faunas. *Journal of the Linnean Society (Zoology)*, 43, 260–282.
- Robinson, P. L. (1973). A problematic reptile from the British Upper Trias. *Journal of the Geological Society of London*, 129, 457–479.
- Romer, A. S. (1956). *Osteology of the reptiles* (p. 772). University of Chicago Press.
- Ruta, M., Cisneros, J. C., Liebrecht, T., Tsuji, L. A., & Müller, J. (2011). Amniotes through major biological crises: Faunal turnover among parareptiles and the end-Permian mass extinction. *Palaeontology*, 54, 1117–1137.
- Säilä, L. K. (2009). Alpha taxonomy of the Russian Permian procolophonoid reptiles. *Acta Palaeontologica Polonica*, 54, 599–608.
- Säilä, L. K. (2010). Osteology of *Leptopleuron lacertinum* Owen, a procolophonoid parareptile from the Upper Triassic of Scotland, with remarks on ontogeny, ecology and affinities. *Earth and Environmental Science Transactions of the Royal Society of Edinburgh*, 101, 1–25.
- Seeley, H. G. (1888). Researches on the structure, organization, and classification of fossil Reptilia. VI. On the anomodont Reptilia and their allies. *Proceedings of the Royal Society of London*, 44, 381–383.
- Silva-Neves, E., Modesto, S. P., & Dias-da-Silva, S. (2020). A new, nearly complete skull of *Procolophon trigoniceps* Owen, 1876 from the Sanga do Cabral Supersequence, Lower Triassic of southern Brazil, with phylogenetic remarks. *Historical Biology*, 32, 574–582.
- Simms, M. J. (1990). Triassic palaeokarst in Britain. *Cave Science*, 17, 93–101.
- Simms, M. J., & Drost, K. (2022). Terrestrial vertebrates from Triassic caves of south-west Britain: older than we thought. The Palaeontological Association 66th Annual Meeting, Programme, Abstracts, AGM Papers 57.
- Skinner, M., Whiteside, D. I., & Benton, M. J. (2020). Late Triassic Island dwarfs? Terrestrial tetrapods of the Ruthin fissure (South Wales, UK) including a new genus of procolophonid. *Proceedings of the Geologists' Association*, 131, 535–561.
- Small, B. J. (1997). A new procolophonid from the Upper Triassic of Texas, with a description of tooth replacement and implantation. *Journal of Vertebrate Paleontology*, 17, 674–678.
- Spencer, P. S. (2000). The braincase structure of *Leptopleuron lacertinum* Owen (Parareptilia, Procolophonidae). *Journal of Vertebrate Paleontology*, 20, 21–30.
- Spencer, P. S., & Benton, M. J. (2000). Procolophonoids from the Permo-Triassic of Russia. In M. J. Benton, E. N. Kurochkin, M. A. Shishkin, & D. M. Unwin (Eds.), *The age of dinosaurs in Russia and Mongolia* (pp. 160–176). Cambridge University Press.
- Spencer, P. S., & Storrs, G. W. (2002). A re-evaluation of small tetrapods from the Middle Triassic Otter Sandstone Formation of Devon, England. *Palaeontology*, 45, 447–467.
- Spiekman, S., Ezcurra, M. D., Butler, R. J., Fraser, N. C., & Maidment, S. C. R. (2021). *Pendraig milnerae*, a new small-sized coelophysoid theropod from the Late Triassic of Wales. *Royal Society Open Science*, 8, 210915.
- Sues, H.-D., & Baird, D. (1998). Procolophonidae (Reptilia: Parareptilia) from the Upper Triassic Wolfville formation of Nova Scotia, Canada. *Journal of Vertebrate Paleontology*, 18, 525–532.
- Sues, H.-D., & Olsen, P. E. (1993). A new procolophonid and a new tetrapod of uncertain, possibly procolophonian affinities from the upper Triassic of Virginia. *Journal of Vertebrate Paleontology*, 13, 282–286.
- Sues, H.-D., Olsen, P. E., Scott, D. M., & Spencer, P. S. (2000). Cranial osteology of *Hypsognathus fenneri*, a latest Triassic procolophonid reptile from the Newark Supergroup of eastern North America. *Journal of Vertebrate Paleontology*, 20, 275–284.
- Sues, H.-D., & Reisz, R. R. (2008). Anatomy and phylogenetic relationships of *Sclerosaurus armatus* (Amniota: Parareptilia) from the Buntsandstein (Triassic) of Europe. *Journal of Vertebrate Paleontology*, 28, 1031–1042.
- Sues, H.-D., & Schoch, R. R. (2023). A new Middle Triassic (Ladinian) trilophosaurid stem-archosaur from Germany increases diversity and temporal range of this clade. *Royal Society Open Science*, 10, 230083.
- Tsuji, L. A. (2018). *Mandaphon nadra*, gen. et sp. nov., a new procolophonid from the Manda Beds of Tanzania. In C. A. Sidor & S. J. Nesbitt (Eds.), *Vertebrate and climatic evolution in the Triassic rift basins of Tanzania and Zambia* (Vol. 37, pp. 80–87). Society of Vertebrate Paleontology Memoir 17.
- Tsuji, L. A., & Müller, J. (2009). Assembling the history of the Parareptilia: Phylogeny, diversification, and a new definition of the clade. *Fossil Record*, 12, 71–81.
- Walkden, G. M., & Fraser, N. C. (1993). Late Triassic fissure sediments and vertebrate faunas: Environmental change and faunal succession at Cromhall, south West Britain. *Modern Geology*, 18, 511–535.
- Walkden, G. M., Fraser, N. C., Simms, M. J., & Simms, M. J. (2021). The age and formation mechanisms of Late Triassic fissure deposits, Gloucestershire, England: Comments on Mussini, G. et al. (2020). Anatomy of a Late Triassic Bristol fissure: Tytherington fissure 2. *Proceedings of the Geologists' Association*, 132, 127–137.
- Whiteside, D. I., & Duffin, C. J. (2017). Late Triassic terrestrial microvertebrates from Charles Moore's 'Microlestes' quarry, Holwell, Somerset, UK. *Zoological Journal of the Linnean Society*, 179, 677–705.
- Whiteside, D. I., Duffin, C. J., Gill, P. G., Marshall, J. E. A., & Benton, M. J. (2016). The Late Triassic and Early Jurassic fissure faunas from Bristol and South Wales: Stratigraphy and setting. *Palaeontologia Polonica*, 67, 257–287.
- Whiteside, D. I., & Marshall, J. E. A. (2008). The age, fauna and palaeoenvironment of the Late Triassic fissure deposits of

Tytherington, south Gloucestershire, UK. *Geological Magazine*, 145, 105–147.

Zaher, M., Coram, R. A., & Benton, M. J. (2019). The Middle Triassic procolophonid *Kapes bentoni*: Computed tomography of the skull and skeleton. *Papers in Palaeontology*, 5, 111–138.

SUPPORTING INFORMATION

Additional supporting information can be found online in the Supporting Information section at the end of this article.

How to cite this article: Butler, R. J., Meade, L. E., Cleary, T. J., McWhirter, K. T., Brown, E. E., Kemp, T. S., Benito, J., & Fraser, N. C. (2023). *Hwiccewyrn trispiculum* gen. et sp. nov., a new leptopleuronine procolophonid from the Late Triassic of southwest England. *The Anatomical Record*, 1–31. <https://doi.org/10.1002/ar.25316>